



Techno-Economic Assessment of Geothermal Resources in the Variscan Basement of the Northern Upper Rhine Graben

Matthis Frey, Jeroen van der Vaart, Kristian Bär, Claire Bossennec, Philippe Calcagno, Chrystel Dezayes, Ingo Sass

► To cite this version:

Matthis Frey, Jeroen van der Vaart, Kristian Bär, Claire Bossennec, Philippe Calcagno, et al.. Techno-Economic Assessment of Geothermal Resources in the Variscan Basement of the Northern Upper Rhine Graben. Natural Resources Research, 2022, 10.1007/s11053-022-10138-4 . hal-03938044

HAL Id: hal-03938044

<https://brgm.hal.science/hal-03938044>

Submitted on 13 Jan 2023

HAL is a multi-disciplinary open access archive for the deposit and dissemination of scientific research documents, whether they are published or not. The documents may come from teaching and research institutions in France or abroad, or from public or private research centers.

L'archive ouverte pluridisciplinaire **HAL**, est destinée au dépôt et à la diffusion de documents scientifiques de niveau recherche, publiés ou non, émanant des établissements d'enseignement et de recherche français ou étrangers, des laboratoires publics ou privés.



Techno-Economic Assessment of Geothermal Resources in the Variscan Basement of the Northern Upper Rhine Graben

Matthis Frey^{1,5}, Jeroen van derVaart,¹ Kristian Bär,² Claire Bossennec,¹ Philippe Calcagno,³ Chrystel Dezayes,³ and Ingo Sass^{1,4}

Received 7 July 2022; accepted 26 October 2022

Deep geothermal energy represents an essential component of the future energy supply because the resources greatly exceed the demand, and the base load capability can compensate for temporal fluctuations in wind and solar power. By far, the largest amount of heat is contained in the crystalline basement, accessible almost everywhere through deep drilling. An interdisciplinary approach for a techno-economic resource assessment was applied to provide stakeholders with a more reliable basis for decision-making in the Northern Upper Rhine Graben. This approach incorporated data from various sources such as boreholes, outcrops, geophysical surveys, geomechanical models, and operating geothermal power plants. Emphasis was placed on resources tied to large-scale fault zones, exhibiting preferential hydraulic properties. Uncertainties in the calculations were quantified using Monte Carlo simulations. The resource base in the basement of the Northern Upper Rhine Graben is about 830 PWh_{th}, of which about 8.2–16.1 PWh_{th} could potentially be extracted with current technologies in enhanced geothermal systems. A comprehensive sensitivity analysis was carried out, examining the economic influence of nine parameters. Considering the reference power plant and the energy prices before the Ukraine war began in February 2022, the geothermal reserves are about 65% of the resources. However, given the massive recent increase in heat and electricity prices, a higher percentage is also possible. Finally, a socio-economic-environmental assessment shows that in the Northern Upper Rhine Graben, geothermal resources largely coincide with favorable conditions at the surface, making the region a preferred target for geothermal utilization.

KEY WORDS: Crystalline basement, Geothermal energy, Techno-economic resource assessment, Monte Carlo simulation, Sensitivity analysis.

¹Department of Geothermal Science and Technology, Institute of Applied Geosciences, Technical University of Darmstadt, Schmittspahnstraße 9, 64287 Darmstadt, Germany.

²GeoThermal Engineering GmbH, An der Raumfabrik 33C, 76227 Karlsruhe, Germany.

³BRGM, 3 Avenue Claude Guillemin, BP 36009 45060 Orléans Cedex, France.

⁴GFZ German Research Centre for Geosciences, Section 4.8: Geoenergy, Telegrafenberg, 14473 Potsdam, Germany.

⁵To whom correspondence should be addressed; e-mail: frey@geo.tu-darmstadt.de

INTRODUCTION

A rapid reduction in greenhouse gas emissions is essential to mitigate the global effects of man-made climate change. To achieve this aim, major parts of the energy supply need to be shifted from fossil fuels to renewable sources in the coming years (IPCC, 2022). Up to now, German governments and investors have focused primarily on wind and solar

power. However, the significant discrepancy between energy supply and demand throughout the year makes the construction of large energy storages necessary (Bär et al., 2015; Bussar et al., 2016; Welsch et al., 2018). In comparison, geothermal energy enables a base-load capable energy supply such that peak loads can be compensated effectively (Tester et al., 2006; Huenges et al., 2013; Stober & Bucher, 2021). In particular for heat supply, where the dependency on fossil energy sources is still very high both in the residential and commercial sectors, there is a considerable need to expand renewables (BMW, 2021), much of which can be covered by deep geothermal power plants (Moeck, 2022). At present, geothermal energy accounts for only a small share of the energy mix in Germany, but the expansion of this technology is essential for a successful energy transition (Bracke & Huenges, 2022).

The Upper Rhine Graben (URG) is an ideal region for geothermal utilization due to the significantly increased temperature gradient and several potential reservoir horizons (Pribnow & Schellschmidt, 2000; Sass et al., 2011; Stober & Bucher, 2015; Freymark et al., 2017). Here, enhanced/engineered geothermal systems (EGS) are generally developed where the permeability of the fractured reservoir is improved by hydro-mechanical and/or hydrochemical stimulation. The reservoir volume is constrained by the hydraulically active fracture network during operation and can be mapped using, e.g., induced seismicity. In total, 17 deep geothermal projects have been implemented in the URG since the late 1970s, seven of which are currently in operation (Bruchsal, Insheim, Landau, Riehen, Rittershoffen, Soultz-sous-Forêts, Weinheim), providing 50 MW_{th} of heat and 10 MW_{el} of electricity (Frey et al., 2022a). Thus, only a small portion of the total geothermal resources are currently being utilized (e.g., Kock & Kaltschmitt, 2012).

While aquifers are the preferred targets of geothermal drilling, such hydrothermal reservoirs hold only about 1% of the total resources (Paschen et al., 2003). In contrast, by far the largest amount of heat is contained in the Variscan basement, which is characterized by very high temperatures and an increased density of fractures and faults in the URG (Genter & Traineau, 1996; Sausse & Genter, 2005; Dezayes et al., 2010; Glaas et al., 2021; Bossennec et al., 2022; Frey et al., 2022b). The fault and fracture network may have reasonable natural permeability or has the potential to be enhanced by stimulation. However, exploration has been subject to significant

uncertainties due to the small number of wells that penetrate the entire sedimentary cover and reach the basement. Moreover, the depth resolution or overall quality of most 2D seismic lines is insufficient to image basement structures accurately.

In the past 2 decades, several studies have been conducted to quantify geothermal resources in the URG basement, but their strong geologic simplification of the basement usually allows only for regional considerations (Paschen et al., 2003; Sass et al., 2011; Kock & Kaltschmitt, 2012; GeORG Projektteam, 2013; Jain et al., 2015). In the framework of the Hessen 3D 2.0 (Bär et al., 2021b) and DGE rollout projects (www.nweurope.eu/dge-rollout), gravity and magnetic data were additionally integrated to develop the most detailed 3D model of the crystalline crust in the Northern URG to date (Frey et al., 2021). These results are combined with comprehensive thermal, petrophysical, geomechanical, and financial information to obtain a refined techno-economic resource assessment. This model provides stakeholders with a valuable basis for decision-making during site and reservoir selection for geothermal drilling. The deep geothermal resources of the sedimentary reservoir horizons in the Northern URG will be covered in a subsequent publication by van der Vaart et al. (in prep.).

GEOLOGICAL FRAMEWORK

The URG is a passive continental rift system that developed from the Eocene onwards due to the changing lithospheric stress field in the alpine foreland (e.g., Ziegler et al., 1995). Both location and orientation of the URG are governed by the reactivation of large fault and shear zones in the basement that formed since the Paleozoic (Schumacher, 2002; Edel et al., 2007; Grimmer et al., 2017). The complex multiphase Cenozoic rift evolution caused a distinct asymmetry both parallel and perpendicular to the strike direction, evident in the significant variations in sediment thickness throughout the URG (e.g., Doebl & Olbrecht, 1974). In the first main rifting phase, crustal extension was dominant, dividing the crust into numerous isolated fault blocks, bounded by large-scale normal faults. During the Miocene, a counterclockwise rotation of σ_{Hmax} led to the reactivation of these faults in a strike-slip or oblique sense (Buchner, 1981; Behrmann et al., 2003; Dèzes et al., 2004). The URG represents a convection-dominated geothermal play system,

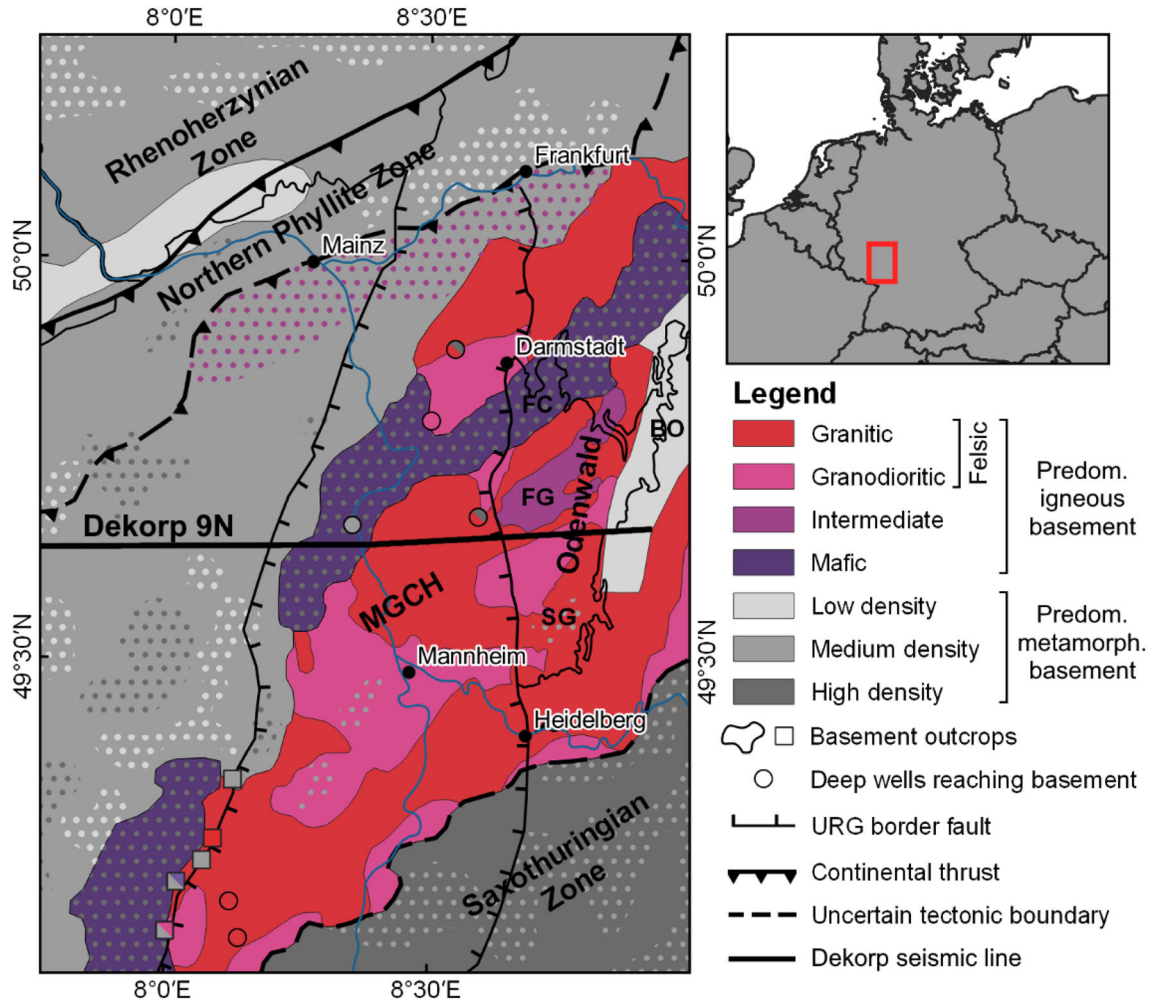


Figure 1. Predictive subcrop map of the Northern URG crystalline basement based on the joint gravity and magnetic inversion of Frey et al. (2021). Dotted signature indicates areas of heterogeneous composition and uncertain interpretation. A detailed image of the fault network in the Northern URG is given in Figure 2. BO Böllsteiner Odenwald, FC Frankenstein complex, FG Flasergranitoid zone, SG Flasergranitoid zone.

where local thermal anomalies mainly result from the upwelling of deep groundwaters along fault zones with increased fracture permeability in the fault damage zones (Moeck, 2014).

The basement architecture in the URG region was mainly established during the Variscan orogeny (Kossmat, 1927; Behr et al., 1984), involving the juxtaposition of Laurussia, Gondwana and several micro-terranes (Armorican Terrane Assemblage) with the main collisional phase during the Carboniferous (e.g., Kroner et al., 2008). In the Northern URG, the Mid-German Crystalline High (MGCH) makes up most of the basement (Fig. 1), which is interpreted as a former active continental margin in the north of Armorican Terrane Assem-

blage (Franke, 2000; Zeh & Gerdes, 2010). The crystalline Odenwald at the northeastern margin of the URG is the largest outcrop of the MGCH and reveals substantial lateral heterogeneity in composition and structure (Krohe & Willner, 1995; Stein, 2001). In the western (Bergsträßer) Odenwald, subduction-related igneous rocks predominate that intruded into meta-volcano and meta-sedimentary host rocks (Krohe, 1991; Altherr et al., 1999). From north (Frankenstein Complex) to south (Southern Plutons) a transition from predominantly mafic to felsic plutonic rocks can be observed. Similarly, the age of the intrusives decreases from about 360 Ma to about 325–330 Ma toward the south (Kreuzer & Harre, 1975; Kirsch et al., 1988; Anthes & Reis-

chmann, 2001). Only a few basement outcrops exist in isolated quarries along the western rift margin, and less than 10 deep wells in the URG reached the basement so far (Fig. 1). However, additional information is provided by gravity and magnetic data, which were used to trace distinct lithologic units hidden beneath the sedimentary cover (for details see Frey et al., 2021).

The MGCH is separated from the Northern Phyllite Zone (NPZ) to the north by a major continental thrust zone (Blundell et al., 1992; Brun et al., 1992), whose location is not precisely known yet. The NPZ, exposed in the southern Taunus and Hunsrück, comprised a tectonic mélange of greenschist-facies meta-sediments and meta-volcanics (Klügel, 1997). To the south, the MGCH merges into the Saxothuringian Zone, which consists of a metamorphic early Paleozoic shelf sequence overlying Neoproterozoic gneiss (Falk et al., 1995).

MATERIAL AND METHODS

3D Model and Parametrization

The resource assessment approach of this study is based on a plausible 3D model of the crystalline basement in the Northern URG. The software Petrel was used to merge existing models, mainly from the GeORG, Hesse 3D and DGE Rollout projects (Sass et al., 2011; GeORG Projektteam, 2013; Bär et al., 2021b; Frey et al., 2021; van der Vaart et al., 2021). Furthermore, additional borehole data and seismic profiles, e.g., the reprocessed DEKORP 9 N line (Homuth et al., 2021), were included. The final model spans over 110 km from north to south, 60 km from east to west, and extends to a depth of 6 km. In previous geothermal potential studies (Paschen et al. 2003; Tester et al. 2006), 10 km was often assumed as the maximum depth of technically feasible utilization, which leads to far too optimistic estimates. In fact, almost no geological data are available below 6 km, preventing any reliable statements about the hydraulic, thermal and geomechanical conditions in this depth range. The 3D model was converted into an irregular grid with a cell size of typically $500 \times 500 \times 500 \text{ m}^3$. At the top of the basement, the cell height varies to handle the anticipated subsurface topography (Fig. 2a) as accurately as possible.

Supplementary to the structural model of the basement, information on the subsurface temperature distribution is essential. Therefore, the Germany-wide temperature model of Agemar et al. (2012) was used (Fig. 2b), which covers both the sedimentary horizons and the basement with a spatial resolution of $2 \times 2 \text{ km}$. The model used data from approximately 10,500 wells of varying quality. A 3D universal kriging approach was applied to calculate the temperature model, providing indications of the measurement and kriging uncertainties. In the basement, where almost no temperature information is available in the model (mostly below 4–5 km depth), a constant temperature increase of $30 \text{ }^\circ\text{C/km}$ was assumed to extrapolate temperature values. This value agrees with observed geothermal gradients below the convection-dominated depth interval, e.g., in Soultz-sous-Forêts (Genter et al., 2010). It should be noted that local convection cells, lithological changes, or fault zones are poorly resolved in this purely interpolative model. However, the measured regional-scale thermal anomalies are well represented. Temperature models with a higher resolution exist for specific parts of the URG (Bär et al., 2021b), but because they do not cover the entire model domain, they were not considered further here. The reference temperature was set to the mean surface temperature issued by the German Weather Service for 1991–2020 (DWD, 2021) (about $11 \text{ }^\circ\text{C}$ in the Northern URG). Additionally, information about the inverted rock density was taken from Frey et al. (2021) (Fig. 2c). Petrophysical data, mainly the specific heat capacity, were adapted from the databases of Bär et al. (2020) and Weinert et al. (2020). Information on the 3D stress tensor in the Northern URG, provided by Ahlers et al. (2021), was used to determine the reactivation potential of fault zones (see details below).

Technical Assessment

The volumetric (‘heat in place’) approach, proposed by Muffler and Cataldi (1978), was adopted in this study and further refined to quantify the geothermal resources of the basement. This rather simplistic method involves a limited number of parameters, allowing the uncertainties to be reasonably quantified. In comparison, assessment schemes based on numerical simulation require several assumptions about the reservoir (properties, pore pressure, temperature, etc.), the well comple-

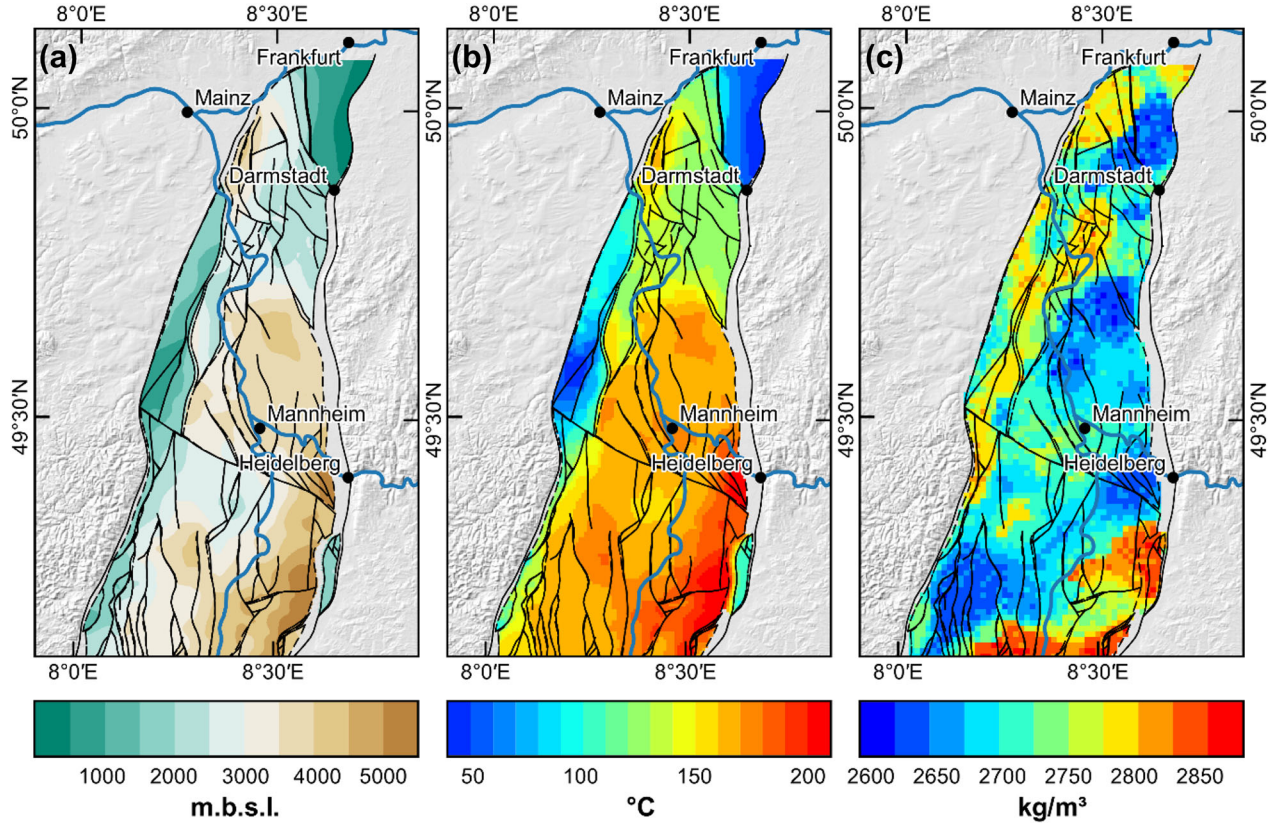


Figure 2. Input data for the geothermal resource assessment: (a) depth of the crystalline basement top including all modeled faults; (b) reservoir temperature at the basement top (based on the temperature model of Agemar et al., 2012); (c) inverted bulk density at the basement top (adapted from Frey et al., 2021).

tion design, the pumping rate, and the operational parameters of the power plant (e.g., Jain et al., 2015). However, especially the hydraulic properties can vary over several orders of magnitude in the basement (Manning & Ingebritsen, 1999; Stober & Bucher, 2007; Achtziger-Zupančič et al., 2017). This makes any simulation result hardly reliable if either the fracture network properties or the local hydraulic parameters are not known from borehole geophysics or hydraulic well testing.

The resource base Q_{total} (J or Wh), also referred to as heat in place or theoretical potential, describes the total amount of thermal energy stored in the Earth's crust (in this case, down to 6 km depth) relative to the ambient surface temperature T_0 (°C). Q_{total} of the individual model cells is calculated as:

$$Q_{\text{total}} = V_{\text{total}} \cdot \rho \cdot c (T_r - T_0) \quad (1)$$

where V_{total} is the volume (m^3) of each model cell, ρ is the rock density (kg/m^3), c is the specific heat

capacity (J/kg/K) and T_r is the reservoir temperature (°C). Due to the fundamentally low porosity of the crystalline basement, the thermal properties of the pore fluid are not regarded.

The geothermal resources Q_{rec} (J or Wh), also known as recoverable heat or technical potential (Muffler and Cataldi, 1978), are defined as the share of the total thermal energy stored in the reservoir that can be extracted considering the current technologies, thus:

$$Q_{\text{rec}} = Q_{\text{total}} \cdot R \quad (2)$$

Consequently, the thermal recovery factor R (unitless) is one of the key factors that influence the potential productivity of geothermal projects. It depends on various parameters, such as the geometry of the reservoir, permeability, reinjection and abandonment temperature (temperature drop in the reservoir at which operation becomes uneconomical), flow rate, and well design (Garg & Combs, 2015; Agemar et al., 2018). The most reliable infor-

mation on the recovery factor is derived from production data of existing geothermal projects. Accordingly, the recovery factor can be as high as 25% for hydrothermal systems (Tester et al., 2006). In fractured reservoirs, R is generally smaller due to the lower permeability. In active geothermal fields in the USA, such as The Geysers, Coso, and Dixie Valley, the recovery factor ranges from about 5–20% (Williams, 2007). In contrast, Grant (2016) reported recovery factors of only 0.2–2% for the research EGS sites Fenton Hill (USA), Rosemanowes (United Kingdom), Hijori (Japan), and Cooper Basin (Australia). Recovery factors from EGS plants in the URG are currently not publicly available. In the present study, a range of R from 0 to 2% is therefore assumed for the base case, i.e., without the influence of large-scale fault zones. The possibility of zero recovery is included in the assessment to account for the risk of too low productivity.

Fault zones in the crystalline basement are generally considered to be effective fluid conduits (Caine et al., 1996; Evans et al., 1997; Bense et al., 2013). A two to three order of magnitude increase in permeability compared to the host rock is primarily observed in the damage zone, which can be several hundred meters wide depending on the displacement. Consequently, an improved heat recovery is expected when targeting major fault zones (e.g., Jolie et al., 2015). Here, a maximum recovery factor of up to 20% was assumed, which is considered the upper limit for fracture-dominated systems (Tester et al., 2006; Williams et al., 2008). Furthermore, the relative location of the fault planes within the regional stress field was taken as a proxy for maximum heat recovery (Agemar et al., 2017). For this purpose, the slip and dilation tendency were calculated for each modeled fault (Morris et al., 1996; Ferrill & Morris, 2003), which were then used as linear weightings for the recovery factor. The slip tendency T_s (Fig. 3a) describes the ratio of the shear stress τ to the normal stress σ_n on a surface (stress components are given in N/m²), thus:

$$T_s = \frac{\tau}{\sigma_n} \quad (3)$$

The dilations tendency T_d (Fig. 3b) is calculated from the normal stress as well as the largest and smallest principal stresses σ_1 and σ_3 , thus:

$$T_d = \frac{\sigma_1 - \sigma_n}{\sigma_1 - \sigma_3} \quad (4)$$

In addition, e.g., Stober and Bucher (2007) showed that the permeability of the basement is strongly dependent on the lithology. They reported results from hydraulic tests in the Black Forest showing that permeability in gneiss can be up to two orders of magnitude lower than in granite under comparable stress conditions. The geomechanical behavior of the foliated metamorphic rocks during reservoir stimulation and production is more complex to predict than for igneous rocks. There is an increased tendency of re-closing fractures, which are formed primarily along the foliation. To account for this, the recovery factor of the metamorphic basement was downweighed by a factor of 0.1 based on the inversion results and interpretations of Frey et al. (2021).

The potential amount of electricity E (J or Wh) that could be generated in the model area is then obtained by multiplying Q_{rec} with the unitless electrical system efficiency η (Beardsmore et al., 2010). A distinction needs to be made between gross and net system efficiency to consider the parasitic electricity consumption of the pumps, thus:

$$E_{\text{gross/net}} = \eta_{\text{gross/net}} \cdot Q_{\text{rec}} \quad (5)$$

According to Eyerer et al. (2020), η_{gross} and η_{net} can be described as a function of the fluid temperature T_{fl} (°C), thus:

$$\eta_{\text{gross}} = 13.59 \cdot \ln(T_{\text{fl}}) - 62.38 \quad (6)$$

$$\eta_{\text{net}} = 13.20 \cdot \ln(T_{\text{fl}}) - 57.60 \quad (7)$$

The mean electrical power output P_{el} (W) of a power plant is calculated by dividing the total gross electricity produced by the project lifetime T_{life} (years) and the annual full load hours h_{full} , thus:

$$P_{\text{el,gross/net}} = \frac{E_{\text{gross/net}}}{T_{\text{life}} \cdot h_{\text{full}}} \quad (8)$$

Monte Carlo Simulation

The resource assessment described above involves several parameters subject to varying degrees of uncertainty. Probability density functions (PDF) can be derived directly from the data basis for some parameters, such as temperature, density, or specific heat capacity. For the recovery factor, ranges of possible values have to be assumed since only a limited database is available (see assumed ranges

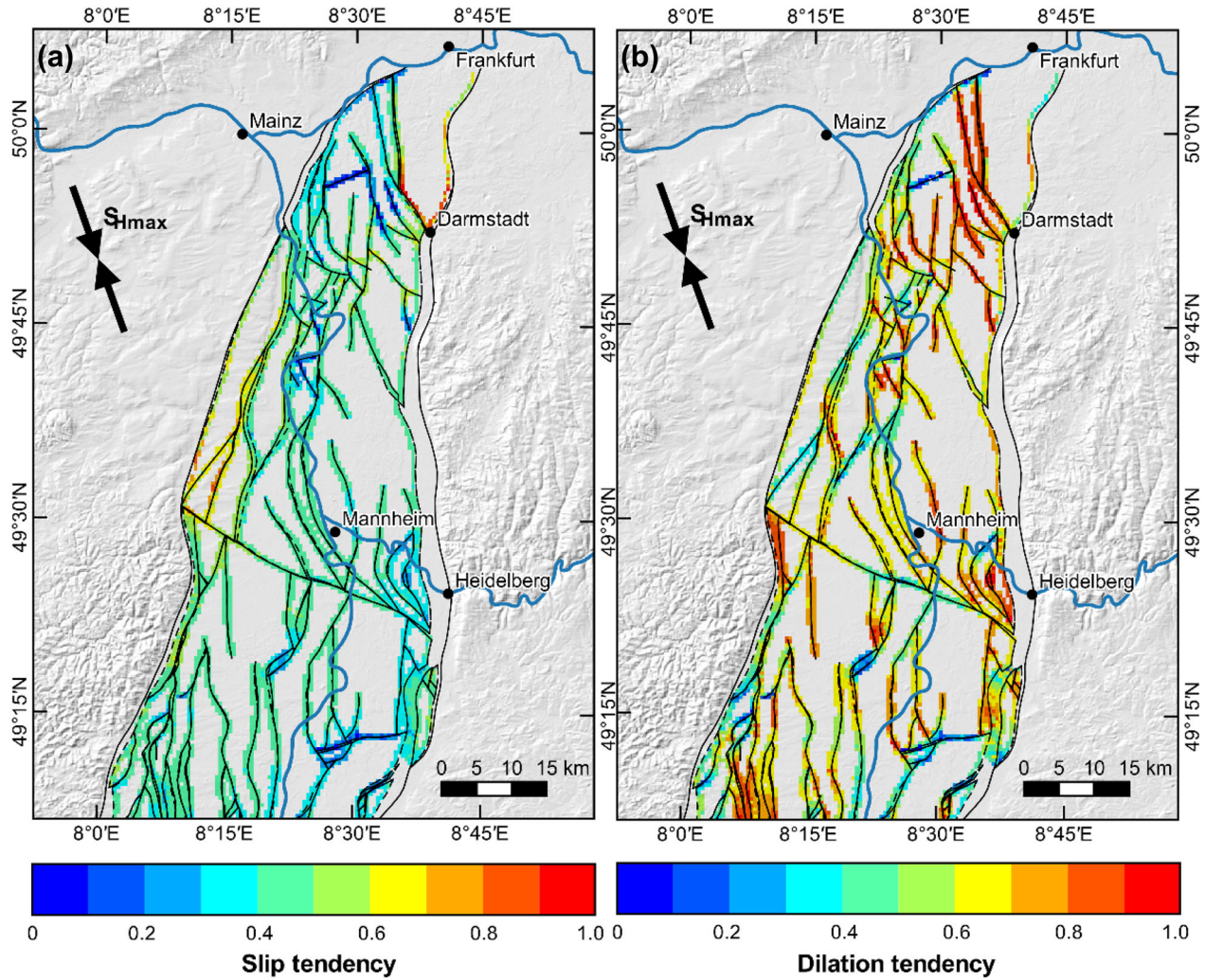


Figure 3. Reactivation potential of fault zones: (a) slip tendency, (b) dilation tendency of modeled faults at the top of the crystalline basement in the Northern URG. Uncertainties of the stress model were not considered.

above). The associated data publication of this study (Frey et al., 2022d) contains the parameterized model used for the calculations, including the standard deviations or ranges of the parameters.

To quantify the risks of geothermal exploration, it is important to combine the individual uncertainties of the input data into a cumulative uncertainty of the target variable. For this purpose, a Monte Carlo simulation was implemented, which is widely used in geosciences (Sambridge & Mosegaard, 2002; Garg & Combs, 2010; Caers, 2011). The basic principle is that random samples of the input parameters are drawn from the previously defined PDFs. The generated values are then used to perform the above-described calculations. This process is re-

peated 100,000 times to obtain a significant distribution, which can then be analyzed statistically.

Economical Assessment

The share of geothermal resources that can be exploited economically at present is referred to as geothermal reserves. These can be determined by comparing the levelized costs of energy (LCOE) with the average revenues earned from the sale of electricity and heat. LCOE describes the ratio of the power plant's net present value (NPV), including the total investment c_{invest} , the operation and maintenance costs $c_{\text{O\&M}}$, and the potential revenues r , to

Table 1. Compilation of economic parameters und costs components of geothermal power plants in the URG. Please note that all costs and revenues refer to the conditions before the war in Ukraine and the corresponding energy price increases. In addition, some of the consulted literature sources are significantly older than 2022, thus it is indicated for which year the prices are valid (€_{year}). For the conversion of prices as of January 2022, the Producer Price Index was used

Item	Costs	Comments	References
<i>Investment costs</i>			
Exploration	1,500,000	In € ₂₀₂₂	
Drill site	1,000,000	In € ₂₀₂₂	
Drilling	$1.198 \cdot e^{0.0004354 \cdot z_{md}}$	In € ₂₀₁₄ per well, Measured depth in m	Schlagermann (2014)
Reservoir stimulation	1,500,000	In € ₂₀₂₂	
Hydraulic Tests	1,000,000	In € ₂₀₂₂	
Well Logging	65 z_{md}	In € ₂₀₁₄ per well, Measured depth in m	Schlagermann (2014)
Submersible pump	1,000,000	In € ₂₀₂₂	
ORC plant	$\begin{cases} 3000 \cdot P_{el} : P_{el} < 3 \text{ MW} \\ 2000 \cdot P_{el} : P_{el} \geq 3 \text{ MW} \end{cases}$	In € ₂₀₂₂ , electrical power In kW	
Combined heat and power generation	Additional 25 % of plant costs	In € ₂₀₂₂	
Seismic monitoring network	1,500,000	In € ₂₀₁₄	Schlagermann (2014)
Public relations	500,000	In € ₂₀₂₂	
Engineering, project management	12% of total investment costs		Adams et al. (2021)
Discount rate	8.25	In %	
Operation and monitoring	3% of investment costs per year		Eyerer et al. (2020)
<i>Revenues</i>			
Feed-in tariff for electricity	0.252 €/kWh	First 20 years of operation	
Market price for electricity	0.071 €/kWh	After 20 years of operation	AEE (2013), Eyerer et al. (2020)
Market price for heat	0.03 €/kWh		Eyerer et al. (2020)

the NPV of the net electricity generated over the project lifetime (Short et al., 1995), thus:

$$LCOE = \frac{\sum_t (C_{invest,t} + C_{O\&M,t} + r_t) \cdot (1 + d)^{-t}}{\sum_t E_{net} \cdot (1 + d)^{-t}} \quad (9)$$

where t is the time step (years) and d the annual effective discount rate (%). Due to the comparatively high risk of geothermal projects, 8.25% was assumed (e.g., Eyerer et al., 2020).

Compilations of the investment costs of geothermal power plants are provided by various sources (Stefánsson, 2002; Sanyal, 2004; Beckers et al., 2014; Limberger et al., 2014; Schlagermann, 2014; Adams et al., 2021). The cost components described therein are in some cases site- and power plant-specific and therefore not directly applicable for each region. To compare data from different years, the Producer Price Index was used to convert prices to be valid for January 2022 (Destatis, 2022b). After consulting with German industry experts (e.g., Menzel 2022), a generalized cost overview was compiled (Table 1). Accordingly, the total invest-

ments consist of the costs for the exploration, the drilling including stimulation, hydraulic tests and geophysical logs, the submersible pump, the power plant at the surface, the management, engineering, planning, and public relations work, the seismological monitoring network, and the insurance of exploration risks. In the following, the major cost elements are discussed in more detail.

Drilling and well completion are the largest cost figures and can reach up to 70% of the total investment for EGS projects. Empirical well cost equations, e.g., published by Legarth (2003), Bloomfield and Laney (2005), Tester et al. (2006), Lukawski et al. (2014) and Schlagermann (2014), generally show an exponential or quadratic increase in cost with depth. For this study, the empirical equation of Schlagermann (2014) was used (Table 1), which focuses on the German market. A simple doublet system with one production well and one injection well was assumed, as this is until now still the standard for EGS projects in the URG. Geothermal wells are usually drilled from one plat-

Table 2. Summary of economic and technical parameter investigated in the sensitivity analysis. Assumed properties of the reference combined heat and power plant are based on operating EGS installations in the URG and worldwide

Parameter	Reference value
Maximum well depth	5 km (TVD)
Lateral reservoir extent	2 km
Recovery factor	Specific for each model cell (see sub-section technical assessment)
Project lifetime	25 years
Full load hours	8000 h/year (electrical), 2000 h/year (thermal)
Investment costs	Specific for each site (see Table 1)
Discount rate	8.25%
Mean heat revenue	0.03 €/kWh
Mean electricity revenue	0.216 €/kWh

form and thus need to be deviated to develop a sufficiently large reservoir volume. The resulting measured depth z_{md} (m) of a well was approximated as:

$$z_{md} = \sqrt{z_{tvd}^2 + s^2} \quad (10)$$

where z_{tvd} is the true vertical depth and s the horizontal distance of the wells (both given in m).

Apart from borehole construction, significant costs are related to surface installations of the power plant. Because the reservoir temperatures are generally below 200 °C in the URG, only binary plants based on the Organic Rankine Cycle (ORC) or Kalina Cycle are applicable. Literature data on the specific costs of binary power plants display a wide range, from about 1000 €/kW to over 5000 €/kW (Rettig et al., 2011; Quoilin et al., 2013; Franco & Vaccaro, 2014; Heberle & Brüggemann, 2015; Lemmens, 2015; Tartière & Astolfi, 2017). However, high values are mainly associated with small ORCs ($\ll 1000$ kW), and costs are expected to decrease with increasing electrical power. A step function was defined accordingly (Table 1). In analogy to the power plant in Landau, an electricity-driven combined heat and power (CHP) process with a power to heat ratio of 0.5 was assumed, in which the residual heat from the ORC can be fed into a district heating network. Such a system additionally requires a heat exchanger and piping. These investments can vary greatly depending on the plant specifications. Thus, additional costs of 25% were estimated for simplification.

While capital expenditures are considered overnight expenses, operation and maintenance costs are recurring annually. They include the costs of personnel, well and surface facility maintenance,

seismic monitoring, and insurance. These amount to about 3% of the total investment costs for EGS projects. Potential revenues arise from the sale of heat from CHP operations.

Sensitivity Analysis

The LCOE and thus the geothermal reserves are influenced by various technical and economic factors. To quantify the respective effect, a comprehensive sensitivity study was conducted. For this purpose, nine parameters were selected and were assumed to have significant impact on the LCOE (Table 2). Based on the experience of existing geothermal projects, values for a reference power plant were defined. These parameters were then varied systematically in equal steps (− 40%, − 20%, + 20%, + 40%). Excluded from this are the well depth and the lateral reservoir extent, as the variation of these parameters is predetermined by the fixed model discretization.

RESULTS

Geothermal Resource Base and Resources

Figure 4a illustrates the total geothermal resource base in the crystalline basement of the Northern URG to a depth of 6 km. The combined heat in place is approximately 830 PWh, with significant spatial variations. While the resource base exceeds 100 TWh per 500×500 m² raster cell at the western and northeastern rift margin, it only ranges from 20 to 40 TWh south of Heidelberg. These variations can be explained primarily by differences

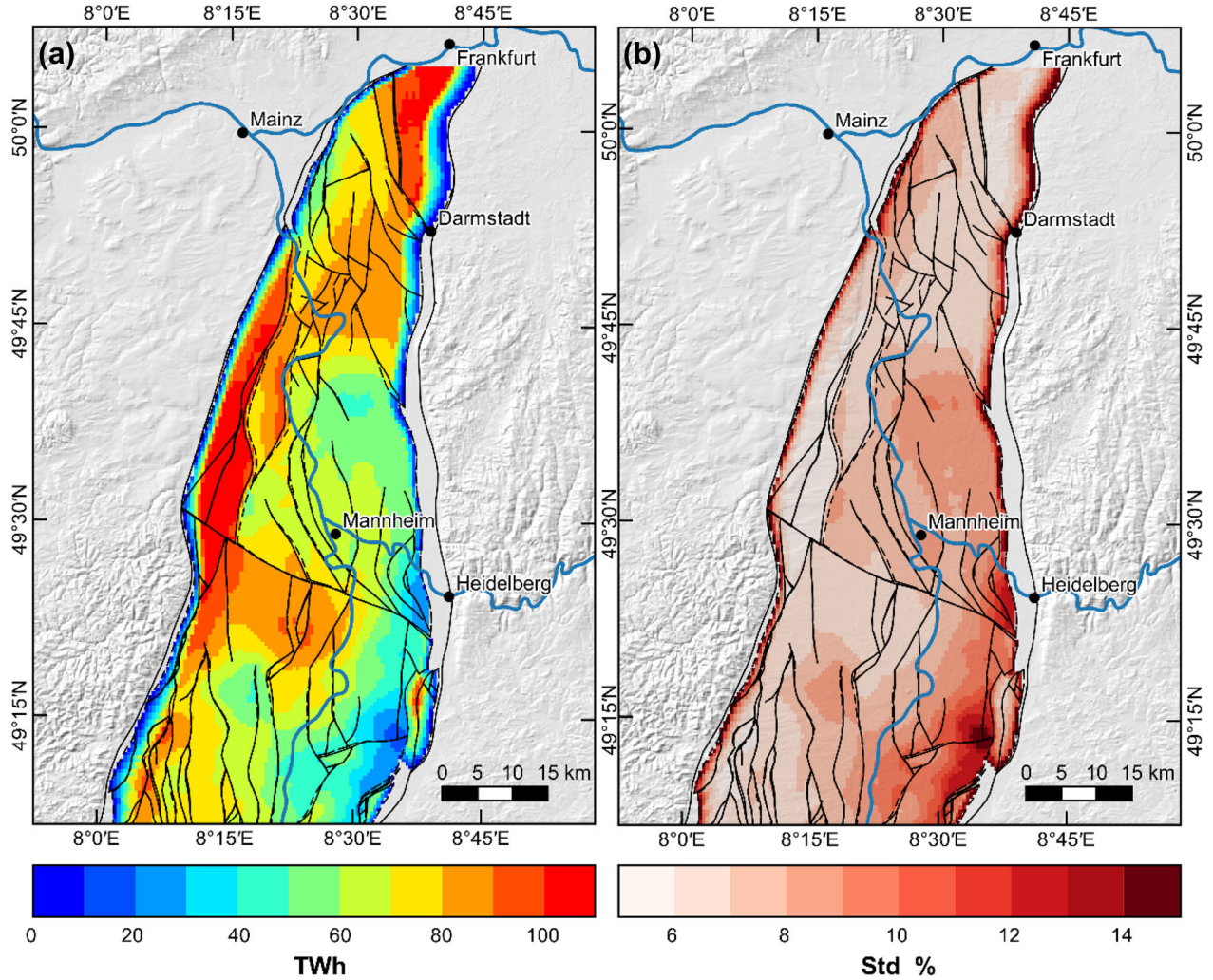


Figure 4. (a) Total geothermal resource base (heat in place) in the crystalline basement down to 6 km depth in the Northern URG (heat per $500 \times 500 \text{ m}^2$ raster cell). (b) Relative standard deviation of the resource base. Note that the geothermal resources of the overlying sedimentary reservoirs are not included.

in the depth to the basement. Accordingly, the thickness of the basement wedge ranges from less than 1 km to more than 5 km within the asymmetric URG (cf. Fig. 2a). The calculation uncertainties are shown as relative standard deviations in Figure 4b. With more than 14%, they are largest at the south-eastern margin of the URG. Here, the greater depth of the basement leads to higher standard deviations of the input parameters and thus also of the calculation result.

To avoid the dominating effect of the varying basement thickness down to 6 km depth, three distinct depth slices (3–4 km, 4–5 km, and 5–6 km) of the geothermal resource base were extracted from

the model (Fig. 5). The heat in place shown therein is primarily dependent on the distribution of temperature and petrophysical properties. In general, the heat content increases with depth as the temperature also increases. Between 3 and 4 km depth, the resource base is very heterogeneously distributed, mainly because the basement is not yet reached or only partially reached at this depth interval in the eastern URG (see Fig. 2). Between 4–5 km and 5–6 km depth, the resource base varies by about $\pm 10\%$ from the average. Consistently high heat in place values are present in the area southwest of Mannheim due to the local positive temperature anomaly.

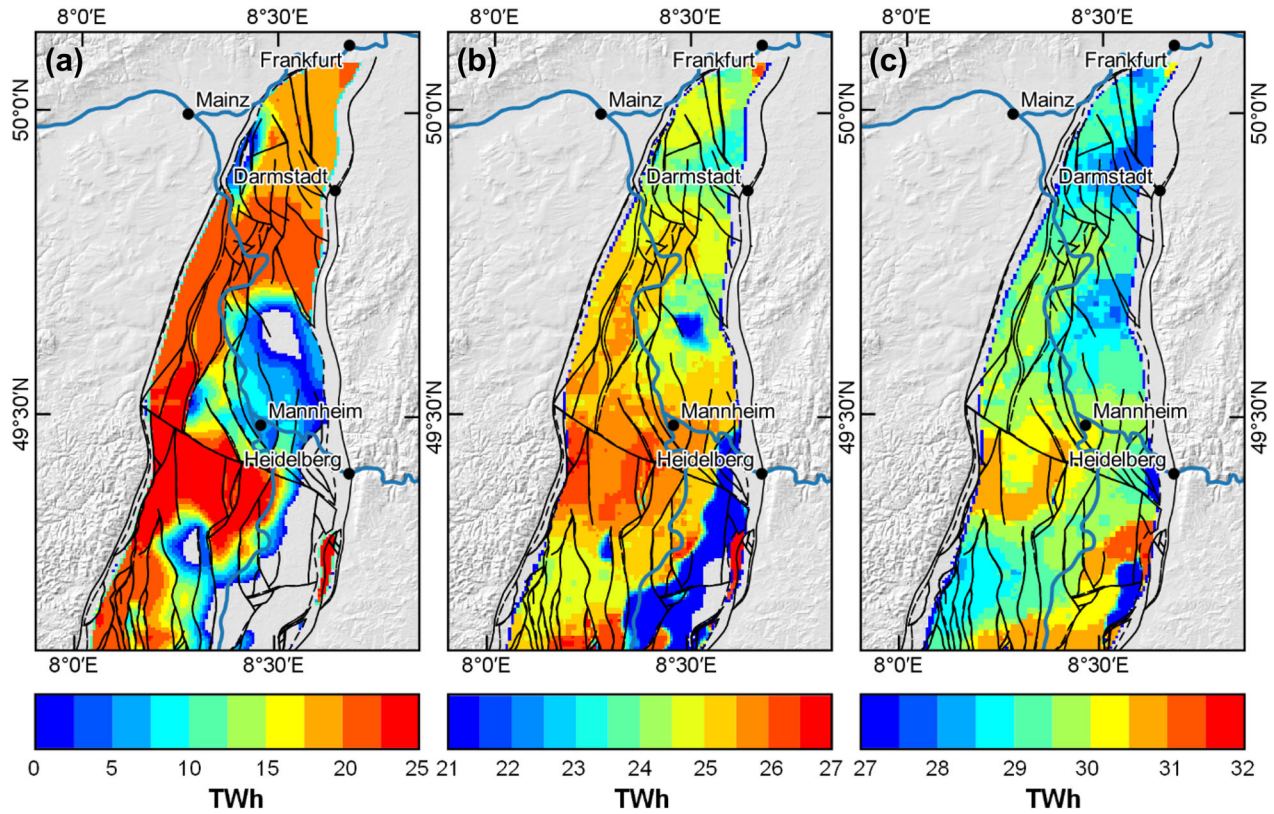


Figure 5. Depth slices of the geothermal resource base (heat in place) in the crystalline basement (heat per $500 \times 500 \text{ m}^2$ raster cell): (a) between 3 and 4 km depth; (b) between 4 and 5 km depth; and (c) between 5 and 6 km depth.

Figure 6 shows three alternative scenarios of potentially recoverable geothermal resources considering the currently available EGS technologies. Scenario A (Fig. 6a) describes the base case, where a maximum R of 2% is assumed for the entire basement, as observed in EGS projects worldwide. The combined resources, in this case, are about $8.2 \text{ PWh}_{\text{th}}$, allowing a net electricity generation of $0.7 \text{ PWh}_{\text{el}}$. The highest values of up to $2 \text{ TWh}_{\text{th}}$ per $500 \times 500 \text{ m}^2$ are again located at the western and northeastern edges of the Northern URG. Scenario B (Fig. 6b) integrates the influence of large-scale fault zones and the regional stress field into the calculation. As a result, the resources amount to about $16.1 \text{ PWh}_{\text{th}}$, with a potential electricity production of $1.3 \text{ PWh}_{\text{el}}$. The highest values of up to 5 TWh per $500 \times 500 \text{ m}^2$ are reached along favorably oriented faults and at fault intersections. The area along the southwestern rift margin exhibits particularly high resources due to the increased fault density and the positive local temperature anomaly.

In addition, there are significant geothermal resources around Mannheim and west of Darmstadt. Scenario C (Fig. 6c) also considered the basement lithology. It was assumed that less favorable hydrogeological conditions characterize the predominantly metamorphic and mafic basement compared to the granitoid basement (Stober & Bucher, 2007). Accordingly, the northwestern and southwestern rift margins are less suitable for deep geothermal exploitation. In this case, the total combined resources are about $9.8 \text{ PWh}_{\text{th}}$, corresponding to a net electricity production of $0.8 \text{ PWh}_{\text{el}}$. The uncertainties are shown as relative standard deviations in Figure 6d–f. The general pattern is similar to Figure 4b, but the standard deviation is substantially higher, ranging from 20 to 60% of the resources. For scenario B, the standard deviation is additionally increased along the modeled fault zones and for scenario C along the boundaries of the major basement units.

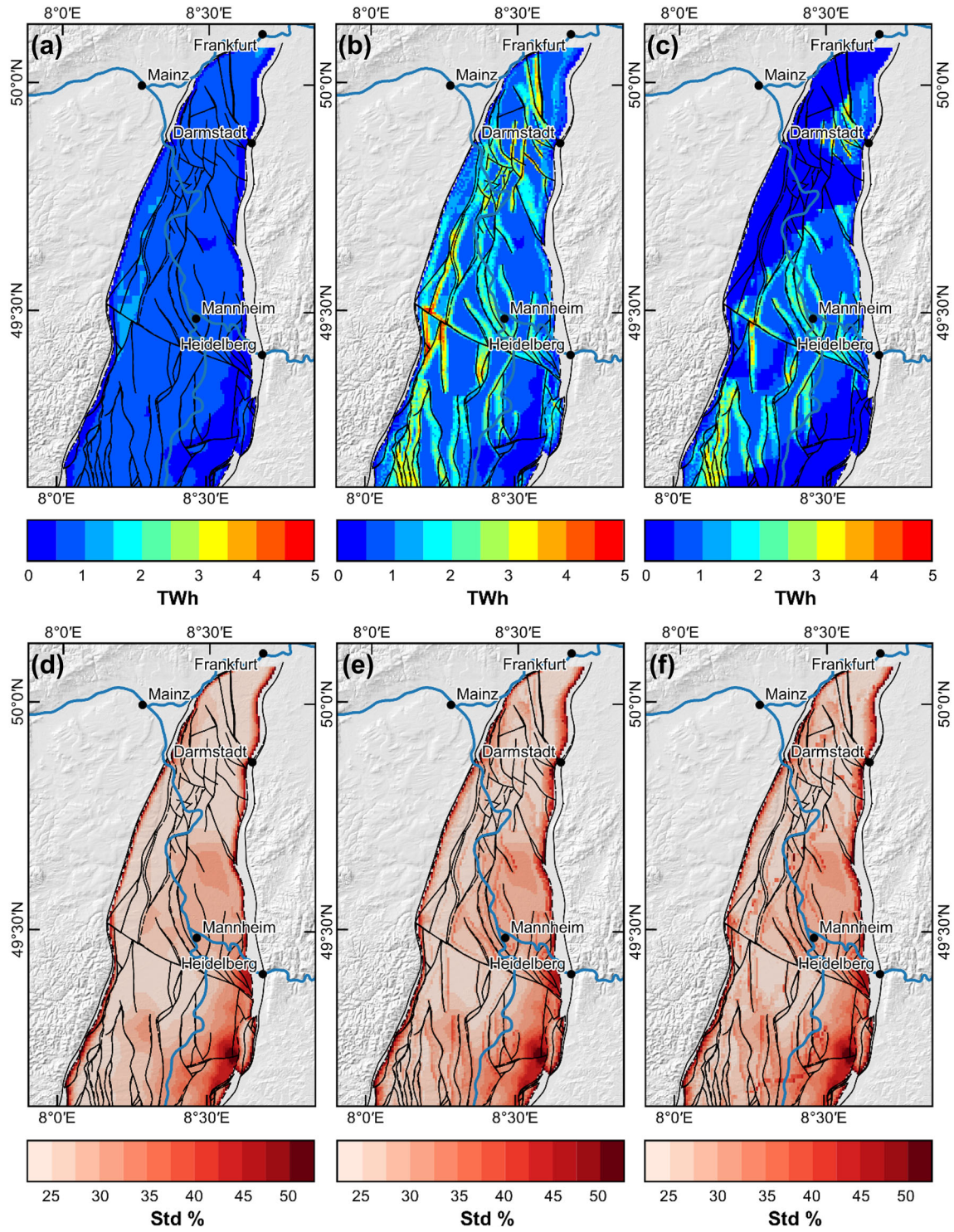


Figure 6. Recoverable geothermal resources in the Northern URG crystalline basement (per $500 \times 500 \text{ m}^2$ raster cell). (a) Scenario A: base case. (b) Scenario B: including the influence of fault zones. (c) Scenario C: including the influence of the basement lithology on hydrogeological properties. (d-f) relative standard deviations of the results.

LCOE and Geothermal Reserves

An economic evaluation was performed based on the calculated recoverable geothermal resources as displayed in Figure 6c and the properties of the reference power plant in Table 2. From this, the cost-supply diagram in Figure 7a is obtained, where the LCOE is plotted against the respective cumulative net electricity production. The curve approaches the geothermal resources for large LCOE. The economically exploitable fraction is obtained by comparing the LCOE with the mean revenues for electricity. Assuming a project lifetime of 25 years (Eyerer et al., 2020), these amount to about 21.6 ct/kWh_{el}, as the feed-in tariff of 25.2 ct/kWh_{el} is paid for 20 years, and afterward a market revenue of about 7.1 ct/kWh_{el} can be expected (AEE, 2013). Accordingly, the geothermal reserves for the reference case amount to about 300 TWh_{el} or 65% of the resources. Note that these assumed revenues are valid for the situation prior to the energy crisis resulting from the Ukraine war. In the first months of 2022, a significant increase in energy prices oc-

curred, but due to the extreme volatility of the market, no reliable forecast of prices can currently be made.

The technical and the economic-financial framework may differ considerably from the reference configuration for specific projects. For this reason, the influence of nine parameters on the LCOE and geothermal reserves was systematically investigated in a sensitivity analysis (Fig. 7b). Detailed cost-supply diagrams for each parameter are given in Figure 8. In general, there is a high degree of agreement with the results of Eyerer et al. (2020), who conducted a similar analysis for hydrothermal reservoirs in Germany.

The maximum drilling depth has the highest positive effect on the total available geothermal resources. It is considered that with deeper wells, also the open hole section becomes longer and therefore more heat can be produced from the reservoir. Furthermore, the fluid temperature increases with depth and thus also the heat content. If the basement is developed to a depth of 6 km instead of 5 km in the entire Northern URG, the reserves are about 110% higher. However, while drilling costs, risk, and technical challenges increase exponentially with depth, the permeability of the basement decreases, making wells deeper than 5 km still rather unlikely in the near future. Recovery factor and the lateral extent of the reservoir, which essentially determine the total amount of heat that a doublet can potentially produce, also positively influence the reserves. They strongly depend, among other factors, on the hydro-mechanical properties of the fracture network, well design, and stimulation effectiveness. A higher recovery factor primarily increases the available recoverable resources and decreases the LCOE, leading to an improved ratio of reserves to resources. The extent of the reservoir does not affect the overall amount of recoverable heat, but with larger reservoir volume, the ratio of reserves to resources increases. Accordingly, geothermal reserves can be significantly increased in the future with improved reservoir enhancement technologies or customized well design patterns with more wells than just the standard doublet and multi-laterals in the reservoir section.

Average electricity revenues during the project period are particularly sensitive to political changes in the energy market. Feed-in tariffs are regularly reassessed, hence reductions are possible in the coming years. Conversely, energy prices are generally very volatile, so electricity revenues can fall or

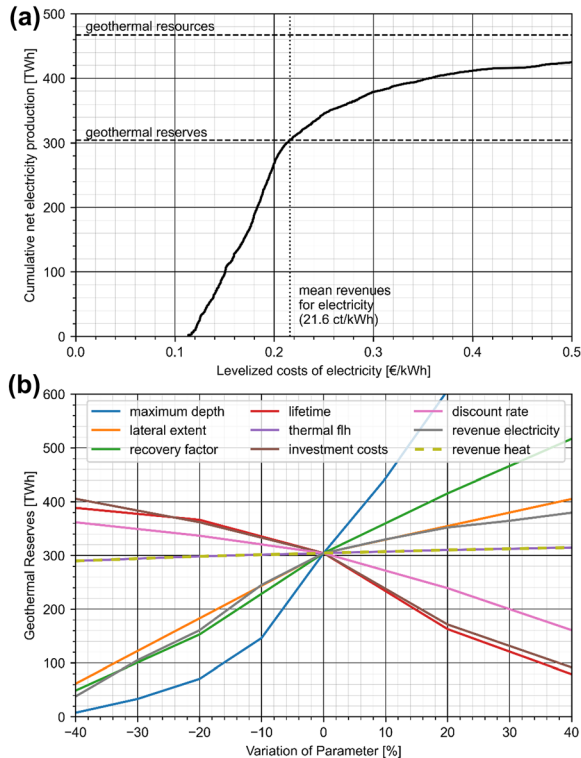


Figure 7. (a) Cost-supply diagram for the reference power plant. (b) Sensitivity analysis of nine factors affecting the total geothermal reserves in the Northern URG crystalline basement. See Table 2 for details of these parameters..

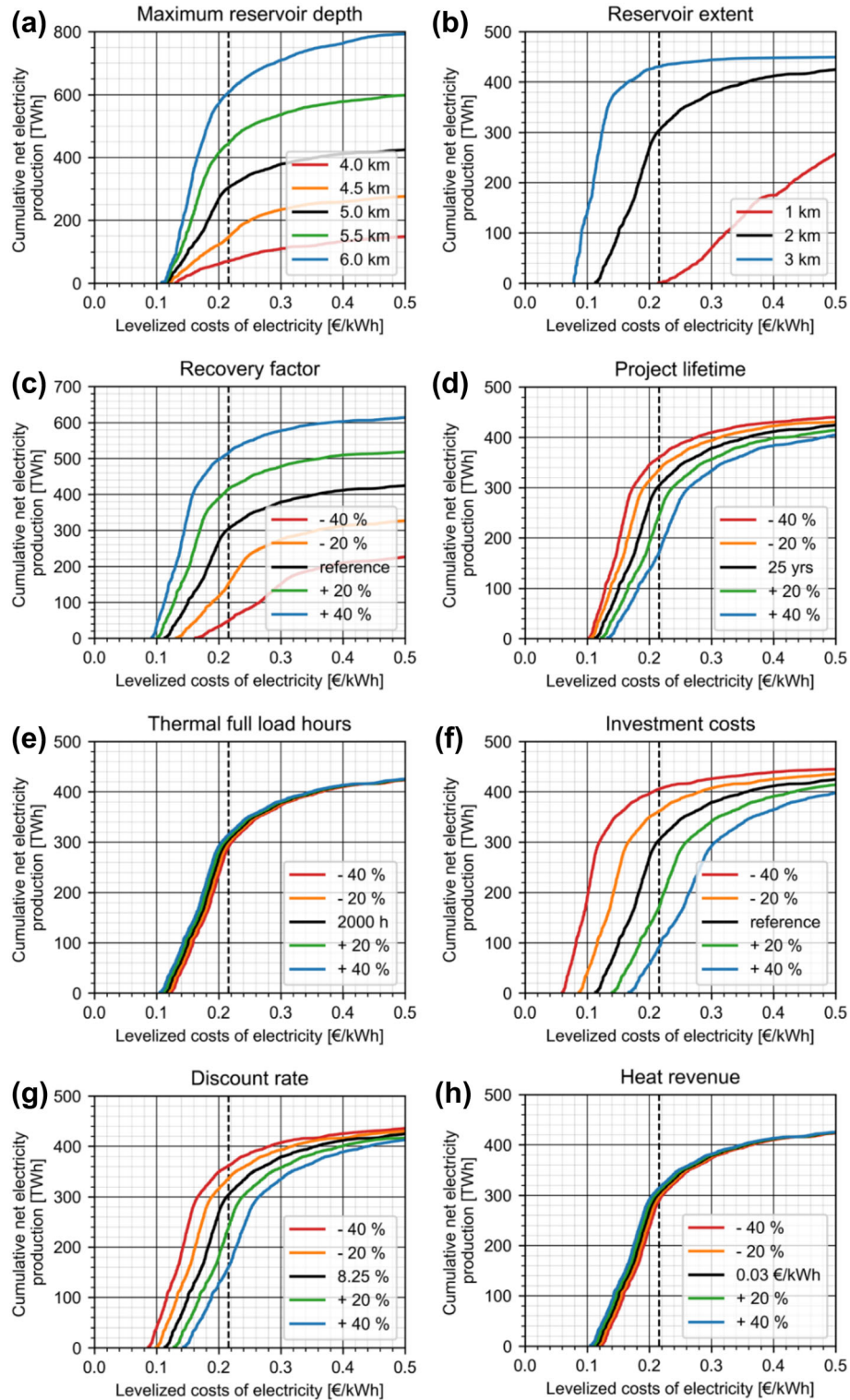


Figure 8. Detailed cost-supply diagrams for eight parameters affecting the electricity production costs and geothermal reserves. The black lines correspond to the reference power plant. The dotted black lines indicate the mean revenue for electricity over the project lifetime of 25 years. No explicit reference values are given for the recovery factor and the investment costs, as they are site-specific.

rise steeply on the free energy market. An increase in average revenues of about 20% would result in about 15% higher reserves, while a 20% decrease would result in 50% lower reserves. In addition, the impact of investment costs is significant. A 20% increase in costs means halving the reserves compared to the reference case. Potentials for cost reductions exist for the ORC and Kalina technologies on the one hand and drilling costs on the other hand.

Interestingly, project lifetime seems to have a similar impact on reserves as investment costs. The reason for this is that with increasing time, the average revenues decrease since feed-in tariffs are only paid for a fixed period. Therefore, from an economic point of view, limiting the project lifetime to 20 years is recommended. The discount rate reflects the risk assessment of geothermal projects. As more power plants are successfully built, this rate may decrease, resulting in lower power production costs and higher reserves. The thermal full load hours and thermal revenues for the assumed power-to-heat ratio of 0.5 only slightly affect the reserves.

DISCUSSION

Limitations of the Volumetric Approach

For the first time, a techno-economic assessment of geothermal resources was carried out for the Variscan basement in the Northern URG, which produced a high-resolution map ($500 \times 500 \text{ m}^2$ cell size) of the resources including uncertainties (Fig. 6). That said, it is important to note that the approach still significantly simplifies the geothermal system. The purely static model neglects all temporal changes in the reservoir during operation, as they are difficult to quantify on the regional scale. This includes the temperature decline during production, the replenishment of the resource by conduction, convection and radiogenic heat production, as well as changes in permeability due to mineral scaling or thermal contraction of the host rock. As a result, the recovery factor is not constant over the project lifetime (Grant, 2018), but reliable data on the temporal behavior in EGS are still rare.

Furthermore, the fracture network properties are excluded from the regional model, which greatly impact the flow rate in geothermal wells and thus affect the profitability of the power plant. A simplified well design was assumed, but depending on the local structural framework, the actual well path

and completion may vary significantly. Finally, the cost components and other properties for deep geothermal power plants compiled in Tables 1 and 2 are also subject to large variations. A sensitivity analysis therefore compared the individual influence on the LCOE and geothermal reserves.

Consequently, the results presented are mainly indicative of areas with high potential for geothermal use and cannot replace a detailed site-specific investigation prior to drilling. The resource maps are an important basis for a first site selection and the planning of tailored exploration measures. In this context, the integration of 3D seismic datasets is crucial to locate all potentially permeable faults by tracing them from sedimentary horizons down into the basement. Additional information for the reservoir characterization can be provided, for example, by electromagnetic and gravity surveys as well as thermal and hydrochemical monitoring (Bär et al., 2021a). Based on a detailed local 3D model, the temporal thermo-hydro-mechanical (THM) processes relevant for the reservoir stimulation and sustainable operation of the geothermal doublet should then be simulated by high-resolution coupled numerical models. Thereby, the petrophysical rock properties can be derived from comprehensive laboratory investigations and corrected for reservoir conditions (e.g., Bär et al., 2020). Hydrogeological properties of the reservoir may be approximated by combining the few hydraulic test data in the crystalline basement with discrete fracture network models (e.g., Koike et al., 2015; Mahmoodpour et al., 2021). Information on the fracture network properties is provided by sparse boreholes (Afshari et al., 2019; Glaas et al., 2021) but more importantly by analog studies (Bossennec et al., 2021; Bossennec et al., 2022; Frey et al., 2022b). Of particular interest is the influence of the fault damage zone thickness and permeability on the productivity of a geothermal doublet, which can be systematically investigated in high-resolution local models. With a better understanding of the hydraulic reservoir characteristics, it is then possible to estimate the time period over which geothermal heat production can potentially be sustained.

Implications for Geothermal Exploration and Utilization

The presented resource assessment demonstrated that the crystalline basement in the Northern

URG is an attractive reservoir for deep geothermal exploitation due to the vast resource base of 830 PWh_{th}. However, only a fraction (8.2–16.1 PWh_{th}) of it is presumably recoverable with currently available technologies. As expected, the largest resources are associated with major fault zones with a high reactivation potential. Note that in some cases, even fault zones with intermediate slip and dilation tendency may exhibit comparatively high permeabilities, as for example, in Bruchsal. Additional indicators for the potential permeability of fault zones are listed by Agemar et al. (2017) but were not further integrated in the regional-scale study. However, these indicators might be of greater use for local exploration when defining potential drilling targets.

Depending on the hydraulic far-field connectivity, reservoir depletion usually progresses faster than heat resupply through pure conduction and radiogenic heat production. Therefore, after the project lifetime, a rest period is required to recharge the geothermal resources for sustainable utilization of the basement. Conservative estimates suggest a period of about 1000 years (Paschen et al., 2003; Eyerer et al., 2020), which would correspond to a maximum annual heat production of about 8–16 TWh_{th}/year. For comparison, the total annual heat demand in the Northern URG is about 30.6 TWh_{th}/year (Strozyk et al., 2021). Pritchett (1998), on the other hand, reports that 90% of the heat will be renewed after three times the production period. Thus, with a 25-year lifetime, an annual heat production of about 80–160 TWh_{th}/year would be possible. Tester et al. (2006) argue that production can be considered renewable if less than 10% of the heat is extracted annually. This corresponds to a maximum heat production of 0.8–1.6 PWh_{th}/year. More precise insights about the sustainability of geothermal energy will only be provided by long-term experience from commercial EGS projects, but the experiences so far show that the reservoirs in the URG are very well connected to the far-field and can thus be quickly recharged by natural brine circulation on a large scale.

The LCOE analysis has shown that about 65% of the geothermal resources in the Northern URG basement could be exploited economically in the reference case (considering the energy price increase in 2022, the percentage is likely to be even higher). This assessment depends on both the reservoir characteristics and specific investments of the power plants. Drilling is the largest cost factor in EGS projects. The more wells are drilled, the more pro-

ven the technologies are and the better the subsurface is explored, resulting in lower risk and shorter drilling times. Therefore, e.g., Limberger et al. (2014) assume that these costs will decrease significantly in the next decades, which is, however, hardly quantifiable. Another way to reduce drilling costs is to drill multiple wells from one drill pad to take advantage of economies of scale. This is particularly useful if a single doublet proves the resources.

Moreover, the effective stimulation of the reservoir plays an essential role. It essentially controls the reservoir volume, the connectivity of the fracture network, and the recovery factor (e.g., Schulte et al., 2010). In this context, the development of novel stimulation methods is required to minimize the induced seismicity (e.g., Amann et al., 2018). In situ experiments addressing these objectives are to be conducted at the planned GeoLaB underground geoscience laboratory on the eastern margin of the URG (Schätzler et al., 2020).

This study investigates an exclusive geothermal utilization of the basement. Additionally, several sedimentary formations in the Northern URG are suitable for deep geothermal exploitation, namely the Permo-Carboniferous, Buntsandstein, Muschelkalk, and Tertiary sandstones. In particular in the eastern rift area, where the resource base in the basement is low (see Fig. 4), these horizons represent the preferred exploration targets. However, their geothermal potential is not further quantified herein but will be the subject of a subsequent publication (van der Vaart et al., in prep.). Some geothermal projects in the URG pursue a multi-reservoir approach, for example, in Insheim, Landau and Rittershoffen, where both sedimentary horizons and the basement are exploited together. This reduces the exploration risk, and a higher flow rate as well as a higher heat production can be achieved at the same drilling depth. Co-production of heat and electricity currently provides the most economic benefit, as the feed-in tariff for electricity is relatively high, and the sale of heat provides an additional revenue stream. For direct use of heat from the basement, the LCOH usually exceed 0.03 €/kWh_{th}, which was higher than average prices in the Northern URG before the Ukraine war. However, as mentioned above, energy prices have increased by up to 90% in the first months of 2022 (Destatis, 2022a), making the direct use of heat from the basement an economically viable solution as of now.

In addition to conventional EGS projects, interest in closed-loop geothermal systems (CLGS)

has increased in recent years, where heat transfer from the reservoir to the working fluid is based solely on conduction (Beckers et al., 2022). Various designs exist in this regard, including coaxial pipes or large subsurface heat exchangers consisting of multiple lateral horizontal wells (Winsloe et al., 2021). These approaches include several advantages in that they are independent of subsurface hydraulic properties, no stimulation is required, less corrosion and scaling occur, and plants can be scaled as required. CLGS can also be retrofitted into existing geothermal, oil, and gas wells. Disadvantages include high drilling costs and comparatively rapid temperature decline during operation. The companies Eavor and GreenFire Energy have already realized initial demonstration projects in North America (Higgins et al., 2019; Toews et al., 2020). Nevertheless, the technical and economic feasibility on a full industrial scale has yet to be proven. In the URG, there is no direct competition to the classical EGS projects since the CLGS target mostly undisturbed rock units, which are not the primary drill sites for open systems.

Socio-economic-environmental Potential

Apart from the geological, technical and financial parameters, the conditions at the surface must always be considered when developing geothermal power plants, as these can have both positive and negative effects on the feasibility of such projects. Frey et al. (2022c) mapped the socio-economic-environmental potential for deep geothermal energy in the URG. The three considered dimensions consist in total of nine individual indicators. The social dimension includes the population-related aspects of population density, heat demand, social level, and acceptance of renewable energy forms. The economic dimension comprises the gross domestic product, the existing district heating network infrastructure and the public debt rate. Finally, the environmental dimension examines the aspects of land access and greenhouse gas emissions. The different quantifiable components were first normalized and then joined into a composite index via an unweighted generalized mean (for a detailed description of the approach see Frey et al., 2022c).

In the Northern URG, the socio-economic-environmental index exhibits a wide distribution (Fig. 9), with a clear trend between urban and rural areas. The highest potential is found in the large

cities and their peripheral districts, which can be attributed to the concentration of population and industry as well as the extensive heat supply infrastructure (e.g., district heating networks of Frankfurt, Darmstadt, Mannheim and Heidelberg). Here, natural and landscape conservation areas can be limiting factors that make access to geothermal resources difficult or in rare cases completely impossible, since drilling below these areas is still possible by deviated wells at sufficient depth. These are mainly concentrated along the Rhine. The more sparsely populated and agriculturally dominated areas west of the Rhine have the lowest overall socio-economic-environmental potential.

The comparison of the recoverable resources and mean LCOE (Fig. 9a, b) with the socio-economic-environmental index (Fig. 9c) reveals a high degree of correlation. In particular in the Rhine-Neckar area, favorable conditions in the subsurface and on the surface are combined. Likewise, the areas along the southwestern margin of the Northern URG and around Darmstadt are positively rated. Although the socio-economic conditions are good in the Frankfurt metropolitan region, the crystalline basement is less suitable for geothermal utilization.

Again, this regional evaluation is mostly indicative for locations with an overall high potential. In particular, the social acceptance of geothermal plants can vary considerably at the local level and depends primarily on the quality of communication and the integration of the population by the project developers. The specific decision-making for a drill site represents a multidimensional problem that has to be solved via analytical hierarchical processes (Raos et al., 2022). This involves carefully weighing the conditions in the subsurface against the conditions at the surface.

CONCLUSIONS

A detailed techno-economic resource assessment was conducted for the crystalline basement in the Northern URG. The following conclusions are drawn from these investigations:

- The Northern URG basement exhibits a vast geothermal resource base of approximately 830 PWh_{th}, of which between 8.2 and 16.1 PWh_{th} are potentially recoverable with current technologies. Geothermal reserves amount to at least

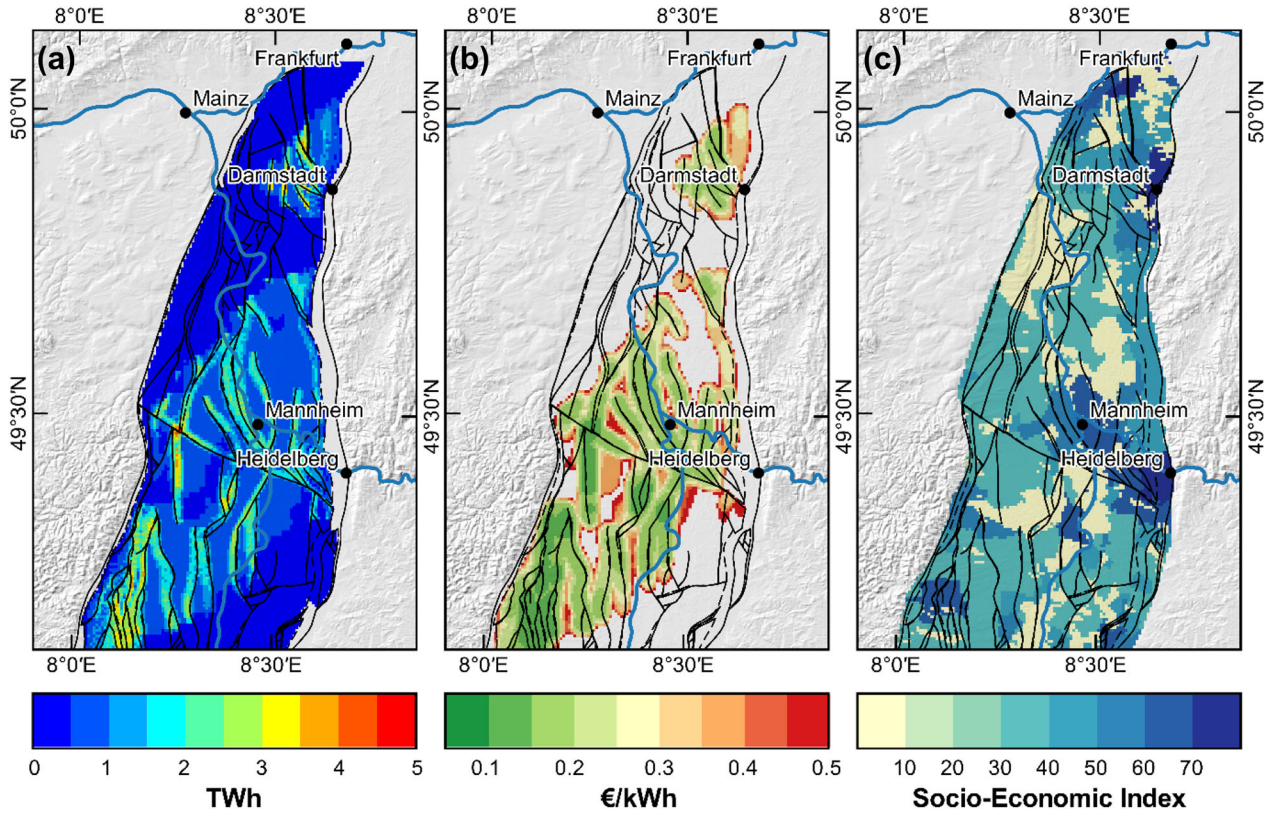


Figure 9. Comparison of (a) the recoverable geothermal resources (per $500 \times 500 \text{ m}^2$ raster cell, Scenario C, see Fig. 6), (b) the LCOE for the reference power plant (see. Table 2) and (c) the socio-economical-environmental potential in the Northern URG. The unitless index ranges from 0 (worst conditions) to 100 (ideal conditions).

65% of the resources. The substantial energy price increases at the beginning of 2022 result in an even higher share of resources that could be used economically. However, due to the energy market volatility, it is currently impossible to make a reliable forecast of price developments.

- The geothermal resources are mainly tied to fault zones with high slip and dilation tendencies located in predominantly granitoid basement units. The largest uncertainties are found along the eastern rift margin, where the top of basement is deepest.
- The impact of various CHP plant properties on the LCOE was investigated using a sensitivity analysis. Significant influences were found for the maximum drilling depth, the recovery factor, the reservoir development, the investment costs, the project lifetime, the discount rate and the average revenue for electricity. In contrast, the thermal full load hours and the average revenue from the sale of heat have a lower significance.
- The socio-economic-environmental potential for

deep geothermal energy reveals a clear urban–rural trend. A comparison with the resources shows a high degree of agreement in the Rhine–Main area, west of Darmstadt, the southeastern areas around Mannheim, and the southwestern rift margin close to Landau

- The techno-economic and socio-economic-environmental analyses are primarily indicative of areas with high potential. They are not a substitute for local targeted exploration activities and multidimensional decision-making processes.
- In-depth studies of the dynamic behavior of reservoir properties during production need to be carried out using local coupled THM models

ACKNOWLEDGMENTS

We thank the three anonymous reviewers for their very helpful comments on this manuscript. The

research was funded by the Interreg NWE Program through the Roll-out of Deep Geothermal Energy in North-West Europe (DGE-ROLLOUT Project, www.nweurope.eu/DGE-Rollout). The Interreg NWE Program is part of the European Cohesion Policy and is financed by the European Regional Development Fund (ERDF). We acknowledge support by the Deutsche Forschungsgemeinschaft (DFG—German Research Foundation) and the Open Access Publishing Fund of Technical University of Darmstadt, through the DEAL project. Petrel was kindly provided by Schlumberger for this research.

FUNDING

Open Access funding enabled and organized by Projekt DEAL.

DATA AVAILABILITY

The discretized and parameterized model used for the geothermal resource assessment can be found in the TUDatalib repository, <https://doi.org/10.48328/tudatalib-898>.

DECLARATIONS

Conflict of Interest The authors have no relevant financial or non-financial interests to disclose.

OPEN ACCESS

This article is licensed under a Creative Commons Attribution 4.0 International License, which permits use, sharing, adaptation, distribution and reproduction in any medium or format, as long as you give appropriate credit to the original author(s) and the source, provide a link to the Creative Commons licence, and indicate if changes were made. The images or other third party material in this article are included in the article's Creative Commons licence, unless indicated otherwise in a credit line to the material. If material is not included in the article's Creative Commons licence and your intended use is not permitted by statutory regulation or exceeds the permitted use, you will need to obtain permission directly from the copyright holder. To view a copy of this licence, visit <http://creativecommons.org/licenses/by/4.0/>.

REFERENCES

- Achtziger-Zupančič, P., Loew, S., & Mariéthoz, G. (2017). A new global database to improve predictions of permeability distribution in crystalline rocks at site scale. *Journal of Geophysical Research: Solid Earth*, 122(5), 3513–3539.
- Adams, B., Ogland-Hand, J., Bielicki, J. M., Schädle, P., & Saar, M. (2021). *Estimating the geothermal electricity generation potential of sedimentary basins using genGEO (the generalizable GEOthermal techno-economic simulator)*. Retrieved 27 June 2022, from <https://doi.org/10.26434/chemrxiv.13514440>.
- AEE. (2013). *Studienvergleich: Entwicklung der Stromgroßhandels- und der CO₂—Zertifikatspreise. Forschungsradar Erneuerbare Energien*. Agentur für Erneuerbare Energien.
- Afshari, M., Valley, B., & Evans, K. (2019). Scaling of fracture patterns in three deep boreholes and implications for constraining fractal discrete fracture network models. *Rock Mechanics and Rock Engineering*, 52(6), 1723–1743.
- Agemar, T., Hese, F., Moock, I., & Stober, I. (2017). Kriterienkatalog für die Erfassung tieferreichender Störungen und ihrer geothermischen Nutzbarkeit in Deutschland. *ZDGG*, 168(2), 285–300.
- Agemar, T., Schellschmidt, R., & Schulz, R. (2012). Subsurface temperature distribution of Germany. *Geothermics*, 44, 65–77. <https://doi.org/10.1016/j.geothermics.2012.07.002>.
- Agemar, T., Weber, J., & Moock, I. (2018). Assessment and public reporting of geothermal resources in Germany: Review and outlook. *Energies*, 11(2), 332. <https://doi.org/10.3390/en11020332>.
- Ahlers, S., Henk, A., Hergert, T., Reiter, K., Müller, B., Röckel, L., Heidbach, O., Morawietz, S., Scheck-Wenderoth, M., & Anikiev, D. (2021). 3D crustal stress state of Germany according to a data-calibrated geomechanical model. *Solid Earth*, 12(8), 1777–1799.
- Altherr, R., Henes-Klaiber, U., Hegner, E., Satir, M., & Langer, C. (1999). Plutonism in the Variscan Odenwald (Germany): From subduction to collision. *International Journal of Earth Sciences*, 88(3), 422–443.
- Amann, F., Gischig, V., Evans, K., Doetsch, J., Jalali, R., Valley, B., Krietsch, H., Dutler, N., Villiger, L., Brixel, B., Klepikova, M., Kittilä, A., Madonna, C., Wiemer, S., Saar, M. O., Loew, S., Driesner, T., Maurer, H., & Giardini, D. (2018). The seismo-hydromechanical behavior during deep geothermal reservoir stimulations: Open questions tackled in a decameter-scale in situ stimulation experiment. *Solid Earth*, 9(1), 115–137.
- Anthes, G., & Reischmann, T. (2001). Timing of granitoid magmatism in the eastern mid-German crystalline rise. *Journal of Geodynamics*, 31(2), 119–143.
- Bär, K., Reinecker, J., Bott, J., Cacace, M., Frey, M., van der Vaart, J., Scheck-Wenderoth, M., Ritter, O., Homuth, B., Fritsche, J.-G., Spath, F., & Sass, I. (2021a). Integrated exploration strategy 'ConvEx' to detect hydrothermal convection in the subsurface. In *Proceedings of the world geothermal congress 2020*. Reykjavik, Iceland.
- Bär, K., Reinsch, T., & Bott, J. (2020). The petrophysical property database (P³)—A global compilation of lab-measured rock properties. *Earth System Science Data*, 12(4), 2485–2515.
- Bär, K., Rühaak, W., Welsch, B., Schulte, D., Homuth, S., & Sass, I. (2015). Seasonal high temperature heat storage with medium deep borehole heat exchangers. *Energy Procedia*, 76, 351–360.
- Bär, K., Schäffer, R., Weinert, S., & Sass, I. (2021b). *Schlussbericht Verbundprojekt "Hessen 3D 2.0": 3D-modell der geothermischen Tiefenpotenziale von Hessen*. Technical University of Darmstadt.

- Beardmore, G. R., Rybach, L., Blackwell, D., & Baron, C. (2010). A protocol for estimating and mapping global EGS potential. *GRC Transactions*, 34, 301–312.
- Beckers, K. F., Lukowski, M. Z., Anderson, B. J., Moore, M. C., & Tester, J. W. (2014). Levelized costs of electricity and direct-use heat from enhanced geothermal systems. *Journal of Renewable and Sustainable Energy*, 6(1), 13141.
- Beckers, K. F., Rangel-Jurado, N., Chandrasekar, H., Hawkins, A. J., Fulton, P. M., & Tester, J. W. (2022). Techno-economic performance of closed-loop geothermal systems for heat production and electricity generation. *Geothermics*, 100, 102318.
- Behr, H.-J., Engel, W., Franke, W., Giese, P., & Weber, K. (1984). The Variscan Belt in Central Europe: Main structures, geodynamic implications, open questions. *Tectonophysics*, 109(1–2), 15–40.
- Behrmann, J. H., Hermann, O., Horstmann, M., Tanner, D. C., & Bertrand, G. (2003). Anatomy and kinematics of oblique continental rifting revealed: A three-dimensional case study of the southeast Upper Rhine graben (Germany). *Bulletin*, 87(7), 1105–1121.
- Bense, V. F., Gleeson, T., Loveless, S. E., Bour, O., & Scibek, J. (2013). Fault zone hydrogeology. *Earth-Science Reviews*, 127, 171–192.
- Bloomfield, K. K., & Laney, P. T. (2005). *Estimating well costs for enhanced geothermal system applications*. Idaho Falls: Idaho National Lab (INL).
- Blundell, D. J., Freeman, R., Mueller, S., & Button, S. (1992). *A continent revealed: The European geotraverse, structure and dynamic evolution*. Cambridge University Press.
- BMWi. (2021). *Zahlen und Fakten: Energiedaten: Nationale und Internationale Entwicklung*. Bundesministerium für Wirtschaft und Energie.
- Bossennec, C., Frey, M., Seib, L., Bär, K., & Sass, I. (2021). Multiscale characterisation of fracture patterns of a crystalline reservoir analogue. *Geosciences*, 11(9), 371.
- Bossennec, C., Seib, L., Frey, M., van der Vaart, J., & Sass, I. (2022). Structural architecture and permeability patterns of crystalline reservoir rocks in the Northern Upper Rhine Graben: Insights from surface analogues of the Odenwald. *Energies*, 15(4), 1310.
- Bracke, R., & Huenges, E. (2022). *Roadmap Tiefengeothermie für Deutschland: Handlungsempfehlungen für Politik*. GFZ Potsdam, Frauenhofer IEG.
- Brun, J. P., Gutscher, M.-A., Teams. (1992). Deep crustal structure of the Rhine Graben from decomp-ecors seismic reflection data: A summary. *Tectonophysics*, 208(1–3), 139–147.
- Buchner, F. (1981). Rhinegraben: Horizontal stylolites indicating stress regimes of earlier stages of rifting. *Tectonophysics*, 73(1–3), 113–118.
- Bussar, C., Stöcker, P., Cai, Z., Moraes, L., Jr., Magnor, D., Wiernes, P., van Bracht, N., Moser, A., & Sauer, D. U. (2016). Large-scale integration of renewable energies and impact on storage demand in a European renewable power system of 2050—Sensitivity study. *Journal of Energy Storage*, 6, 1–10.
- Caers, J. (2011). *Modeling uncertainty in the earth sciences*. Wiley.
- Caine, J. S., Evans, J. P., & Forster, C. B. (1996). Fault zone architecture and permeability structure. *Geology*, 24(11), 1025–1028.
- Destatis. (2022a). *Daten zur Energiepreisentwicklung—Lange Reihen bis April 2022a*. Statistisches Bundesamt. Retrieved 15 June 2022a, from <https://www.destatis.de/DE/Themen/Wirtschaft/Preise/Publikationen/Energiepreise/energiepreisentwicklung-pdf-5619001.html>.
- Destatis. (2022b). *Erzeugerpreisindex gewerblicher Produkte*. Statistische Bundesamt. Retrieved 10 Feb 2022b, from https://www.destatis.de/DE/Themen/Wirtschaft/Preise/Erzeugerpreisindex-gewerbliche-Produkte/_inhalt.html.
- Dezayes, C., Genter, A., & Valley, B. (2010). Structure of the low permeable naturally fractured geothermal reservoir at Soultz. *Comptes Rendus Geoscience*, 342(7–8), 517–530.
- Dèzes, P., Schmid, S. M., & Ziegler, P. A. (2004). Evolution of the European Cenozoic Rift System: Interaction of the Alpine and Pyrenean orogens with their foreland lithosphere. *Tectonophysics*, 389(1–2), 1–33.
- Doebel, F., & Olbrecht, W. (1974). An isobath map of the Tertiary base in the Rhinegraben. In J. H. Illies & K. Fuchs (Eds.), *Approaches to taphrogenesis* (pp. 71–72). Schweizerbart.
- DWD. (2021). *Mean air temperature in Germany between 1991 and 2020*. Deutscher Wetterdienst. Retrieved 27 June 2022, from https://opendata.dwd.de/climate_environment/CDC/griids_germany/multi_annual/air_temperature_mean/.
- Edel, J. B., Schulmann, K., & Rotstein, Y. (2007). The Variscan tectonic inheritance of the Upper Rhine Graben: Evidence of reactivations in the Lias, Late Eocene-Oligocene up to the recent. *International Journal of Earth Sciences*, 96(2), 305–325.
- Evans, J. P., Forster, C. B., & Goddard, J. V. (1997). Permeability of fault-related rocks, and implications for hydraulic structure of fault zones. *Journal of structural Geology*, 19(11), 1393–1404.
- Eyerer, S., Schifflachner, C., Hofbauer, S., Bauer, W., Wieland, C., & Spliethoff, H. (2020). Combined heat and power from hydrothermal geothermal resources in Germany: An assessment of the potential. *Renewable and Sustainable Energy Reviews*, 120, 109661.
- Falk, F., Franke, W., & Kurze, M. (1995). Stratigraphy. In R. D. Dallmeyer, W. Franke, & K. Weber (Eds.), *Pre-Permian geology of central and eastern Europe* (pp. 221–234). Springer.
- Ferrill, D. A., & Morris, A. P. (2003). Dilational normal faults. *Journal of Structural Geology*, 25(2), 183–196.
- Franco, A., & Vaccaro, M. (2014). A combined energetic and economic approach for the sustainable design of geothermal plants. *Energy Conversion and Management*, 87, 735–745.
- Franke, W. (2000). The mid-European segment of the Variscides: Tectonostratigraphic units, terrane boundaries and plate tectonic evolution. *Geological Society, London, Special Publications*, 179, 35–61.
- Frey, M., Bär, K., Stober, I., Reinecker, J., van der Vaart, J., & Sass, I. (2022a). Assessment of deep geothermal research and development in the Upper Rhine Graben. *Geothermal Energy*, 10(18), 1–67.
- Frey, M., Bossennec, C., Seib, L., Bär, K., Schill, E., & Sass, I. (2022b). Interdisciplinary fracture network characterization in the crystalline basement: A case study from the Southern Odenwald, SW Germany. *Solid Earth*, 13(6), 935–955.
- Frey, M., van der Vaart, J., Bär, K. (2022c). *Socio-economic potential mapping for deep geothermal energy in the Upper Rhine Graben: Report WP T1—2.3: DGE-rollout project*. TU Darmstadt.
- Frey, M., van der Vaart, J., Bär, K., Bossennec, C., Calcagno, P., Dezayes, C., & Sass, I. (2022d). *Geothermal resource model of the northern Upper Rhine Graben crystalline basement*. TUdataLib. Retrieved 27 June 2022c, from <https://doi.org/10.48328/tudatalib-898>.
- Frey, M., Weinert, S., Bär, K., van der Vaart, J., Dezayes, C., Calcagno, P., & Sass, I. (2021). Integrated 3D geological modelling of the northern Upper Rhine Graben by joint inversion of gravimetry and magnetic data. *Tectonophysics*, 813, 228927.
- Freymark, J., Sippel, J., Scheck-Wenderoth, M., Bär, K., Stiller, M., Fritsche, J.-G., & Kracht, M. (2017). The deep thermal field of the Upper Rhine Graben. *Tectonophysics*, 694, 114–129.
- Garg, S. K., & Combs, J. (2010). Appropriate use of USGS vulcanometric “heat in place” method and Monte Carlo calcu-

Techno-Economic Assessment of Geothermal Resources

- lations. In *Proceedings of the thirty-fourth workshop on geothermal reservoir engineering*. Stanford, California.
- Garg, S. K., & Combs, J. (2015). A reformulation of USGS volumetric “heat in place” resource estimation method. *Geothermics*, 55, 150–158. <https://doi.org/10.1016/j.geothermics.2015.02.004>.
- Genter, A., Evans, K., Cuenot, N., Fritsch, D., & Sanjuan, B. (2010). Contribution of the exploration of deep crystalline fractured reservoir of Soultz to the knowledge of enhanced geothermal systems (EGS). *Comptes Rendus Geoscience*, 342(7–8), 502–516.
- Genter, A., & Traineau, H. (1996). Analysis of macroscopic fractures in granite in the HDR geothermal well EPS-1, Soultz-sous-Forêts, France. *Journal of Volcanology and Geothermal Research*, 72(1–2), 121–141.
- GeORG Projektteam. (2013). *Geopotenziale des tieferen Untergrundes im Oberrheingraben: Fachlich-Technischer Abschlussbericht des INTERREG-Projekts GeORG*. Freiburg i.Br./Mainz/Strasbourg/Basel.
- Glaas, C., Vidal, J., & Genter, A. (2021). Structural characterization of naturally fractured geothermal reservoirs in the central Upper Rhine Graben. *Journal of Structural Geology*, 148, 104370.
- Grant, M. A. (2016). Physical performance indicators for HDR/EGS projects. *Geothermics*, 63, 2–4.
- Grant, M. A. (2018). Integrated exploration strategy ‘ConvEx’ to detect hydrothermal convection in the subsurface. In *Proceedings of the 43rd workshop on geothermal reservoir engineering Stanford University*. Stanford, California.
- Grimmer, J. C., Ritter, J. R. R., Eisbacher, G. H., & Fielitz, W. (2017). The Late Variscan control on the location and asymmetry of the Upper Rhine Graben. *International Journal of Earth Sciences*, 106(3), 827–853.
- Heberle, F., & Brüggemann, D. (2015). Thermo-economic evaluation of organic Rankine cycles for geothermal power generation using zeotropic mixtures. *Energies*, 8(3), 2097–2124.
- Higgins, B., Muir, J., Scherer, J., & Amaya, A. (2019). GreenFire energy closed-loop geothermal demonstration at the Coso geothermal field. *GRC Transactions*, 43, 434–448.
- Homuth, B., Bär, K., Weinert, S., & Sass, I. (2021). Reprocessing of the hessian DEKORP seismic profiles. In *Tagungsband des 81. Jahrestagung der Deutschen Geophysikalischen Gesellschaft*, Kiel.
- Huenges, E., Kohl, T., Kolditz, O., Bremer, J., Scheck-Wenderoth, M., & Vienken, T. (2013). Geothermal energy systems: Research perspective for domestic energy provision. *Environmental Earth Sciences*, 70(8), 3927–3933.
- IPCC. (2022). *Working Group III contribution to the IPCC sixth assessment report (AR6-WG3)*.
- Jain, C., Vogt, C., & Clauser, C. (2015). Maximum potential for geothermal power in Germany based on engineered geothermal systems. *Geotherm Energy*, 3(1), 1–20.
- Jolie, E., Moeck, I., & Faulds, J. E. (2015). Quantitative structural–geological exploration of fault-controlled geothermal systems—A case study from the Basin-and-Range Province, Nevada (USA). *Geothermics*, 54, 54–67.
- Kirsch, H., Kober, B., & Lippolt, H. J. (1988). Age of intrusion and rapid cooling of the Frankenstein gabbro (Odenwald, SW-Germany) evidenced by $^{40}\text{Ar}/^{39}\text{Ar}$ and single-zircon $^{207}\text{Pb}/^{206}\text{Pb}$ measurements. *International Journal of Earth Sciences*, 77(3), 693–711.
- Klügel, T. (1997). *Geometrie und Kinematik einer variszischen Plattengrenze: der Südrand des Rhenoherzynikums im Taunus*. Hessisches Landesamt für Bodenforschung.
- Kock, N., & Kaltschmitt, M. (2012). Geothermisch erschließbare Niedertemperaturwärmesenken in Deutschland—Identifikation und Quantifizierung. *Zeitschrift für Energiewirtschaft*, 36(3), 191–203.
- Koike, K., Kubo, T., Liu, C., Masoud, A., Amano, K., Kurihara, A., Matsuo, T., & Lanyon, B. (2015). 3D geostatistical modeling of fracture system in a granitic massif to characterize hydraulic properties and fracture distribution. *Tectonophysics*, 660, 1–16.
- Kossmat, F. (1927). Gliederung des varistischen Gebirgsbaues. *Abhandlungen Sächsischen Geologischen Landesamts*, 1, 1–39.
- Kreuzer, H., & Harre, W. (1975). K/Ar-altersbestimmungen an hornblenden und biotiten des kristallinen Odenwalds. In G. C. Amstutz, S. Meisl, & E. Nickel (Eds.), *Mineralien und gesteine im Odenwald* (pp. 70–78). Heidelberg.
- Krohe, A. (1991). Emplacement of synkinematic plutons in the Variscan Odenwald (Germany) controlled by transtensional tectonics. *International Journal of Earth Sciences*, 80(2), 391–409.
- Krohe, A., & Willner, A. P. (1995). IV.C.2 the Odenwald crystalline complex. In R. D. Dallmeyer, W. Franke, & K. Weber (Eds.), *Pre-permian geology of central and eastern Europe* (pp. 182–185). Berlin Heidelberg: Springer.
- Kroner, U., Mansy, J. L., Mazur, S., Aleksandrowski, P., Hann, H. P., & Huckriede, H. (2008). Variscan tectonics. In T. McCann (Ed.), *The geology of central Europe: Volume 1: Precambrian and palaeozoic* (pp. 599–664). Geological Society of London.
- Legarth, B. A. (2003). *Erschließung sedimentärer Speichergesteine für eine geothermische Stromerzeugung: Scientific technical report STR03/09*. GFZ German Research Centre for Geosciences.
- Lemmens, S. (2015). A perspective on costs and cost estimation techniques for organic rankine cycle systems. In *Proceedings of the 3rd international seminar on ORC power systems (ASME ORC 2015)*, Brussels, Belgium.
- Limberger, J., Calcagno, P., Manzella, A., Trumphy, E., Boxem, T., Pluymaekers, M. P. D., & van Wees, J.-D. (2014). Assessing the prospective resource base for enhanced geothermal systems in Europe. *Geothermal Energy Science*, 2(1), 55–71.
- Lukawski, M. Z., Anderson, B. J., Augustine, C., Capuano, L. E., Beckers, K. F., Livesay, B., & Tester, J. W. (2014). Cost analysis of oil, gas, and geothermal well drilling. *Journal of Petroleum Science and Engineering*, 118, 1–14.
- Mahmoodpour, S., Singh, M., Turan, A., Bär, K., & Sass, I. (2021). Hydro-thermal modeling for geothermal energy extraction from Soultz-sous-Forêts, France. *Geosciences*, 11(11), 464.
- Manning, C. E., & Ingebritsen, S. E. (1999). Permeability of the continental crust: Implications of geothermal data and metamorphic systems. *Reviews of Geophysics*, 37(1), 127–150.
- Moeck, I. (2022). *Metastudie zur nationalen Erdwärmestrategie: Ersatz fossiler Brennstoffe im Bereich Raumwärme und Warmwasser durch Geothermie als unverzichtbarer Bestandteil im Energiesektor Ökonomie bis 2045*. Leibniz-Institut für Angewandte Geophysik, Hannover.
- Moeck, I. S. (2014). Catalog of geothermal play types based on geologic controls. *Renewable and Sustainable Energy Reviews*, 37, 867–882.
- Morris, A., Ferrill, D. A., & Brent Henderson, D. (1996). Slip-tendency analysis and fault reactivation. *Geology*, 24(3), 275.
- Muffler, P., & Cataldi, R. (1978). Methods for regional assessment of geothermal resources. *Geothermics*, 7(2–4), 53–89.
- Paschen, H., Ortel, D., & Grünwald, R. (2003). *Möglichkeiten geothermischer Stromerzeugung in Deutschland: Sachstandsbericht*. Büro für Technikfolgen-Abschätzung beim Deutschen Bundestag.
- Pribnow, D., & Schellschmidt, R. (2000). Thermal tracking of upper crustal fluid flow in the Rhine Graben. *Geophysical Research Letters*, 27(13), 1957–1960.
- Pritchett, J. W. (1998). Modeling post-abandonment electrical capacity recovery for a two-phase geothermal reservoir. *Geothermal Resources Council Transaction*, 22, 521–528.

- Quoilin, S., van den Broek, M., Declaye, S., Dewallef, P., & Lemort, V. (2013). Techno-economic survey of Organic Rankine Cycle (ORC) systems. *Renewable and Sustainable Energy Reviews*, 22, 168–186.
- Raos, S., Hranić, J., Rajšl, I., & Bär, K. (2022). An extended methodology for multi-criteria decision-making process focused on enhanced geothermal systems. *Energy Conversion and Management*, 258, 115253.
- Rettig, A., Lagler, M., Lamare, T., Li, S., Mahadea, V., McCallion, S., & Chernushevich, J. (2011). Application of organic Rankine cycles (ORC). In *Proceedings of the world engineer's convention*. Geneva, Switzerland.
- Sambridge, M., & Mosegaard, K. (2002). Monte Carlo Methods in geophysical inverse problems. *Reviews of Geophysics*, 40(3), 1–29.
- Sanyal, S.K. (2004). Cost of geothermal power and factors that affect it. In *Proceedings of the Twenty-Ninth Workshop on Geothermal Reservoir Engineering*, Stanford, California. 26–28. January.
- Sass, I., Hoppe, A., Arndt, D., & Bär, K. (2011). *Forschungs-und Entwicklungsprojekt 3D Modell der Geothermischen Tiefenpotenziale von Hessen: Abschlussbericht*. TU Darmstadt.
- Sausse, J., & Genter, A. (2005). Types of permeable fractures in granite. *Geological Society, London, Special Publications*, 240(1), 1–14.
- Schätzler, K., Bremer, J., Schill, E., Kohl, T., Kühn, M., Kolditz, O., Sass, I. (2020). GeoLaB – Das geowissenschaftliche Zukunftsprojekt für Deutschland. Mining Report Glückauf. <https://mining-report.de/geolab-das-geowissenschaftliche-zukunftsprojekt-fuer-deutschland/>.
- Schlagerrmann, P. (2014). *Exergoökonomische analyse geothermischer strombereitstellung am beispiel des oberrheingrabens*. PhD Thesis. TU München.
- Schulte, T., Zimmermann, G., Vuataz, F., Portier, S., Tischner, T., Junker, R., Jatho, R., & Huenges, E. (2010). Enhancing geothermal reservoirs. In E. Huenges (Ed.), *Geothermal energy systems* (pp. 173–243). Wiley.
- Schumacher, M. E. (2002). Upper Rhine Graben: Role of pre-existing structures during rift evolution. *Tectonics*, 21(1), 1–17.
- Short, W., Packey, D. J., & Holt, T. (1995). *A manual for the economic evaluation of energy efficiency and renewable energy technologies*. National Renewable Energy Lab (NREL).
- Stefánsson, V. (2002). Investment cost for geothermal power plants. *Geothermics*, 31(2), 263–272.
- Stein, E. (2001). The geology of the Odenwald crystalline complex. *Mineralogy and Petrology*, 72(1–3), 7–28.
- Stober, I., & Bucher, K. (2007). Hydraulic properties of the crystalline basement. *Hydrogeology Journal*, 15(2), 213–224.
- Stober, I., & Bucher, K. (2015). Hydraulic and hydrochemical properties of deep sedimentary reservoirs of the Upper Rhine Graben, Europe. *Geofluids*, 15(3), 464–482.
- Stober, I., & Bucher, K. (2021). *Geothermal energy: From theoretical models to exploration and development*. Springer.
- Strozyk, F., Herbst, E., & Khashfe, E. (2021). *Map of the spatial distribution of the heat demand at the surface: Report WP T1—2.1: DGE-Rollout Project*. Fraunhofer IEG.
- Tartière, T., & Astolfi, M. (2017). A world overview of the organic Rankine cycle market. *Energy Procedia*, 129, 2–9. <https://doi.org/10.1016/j.egypro.2017.09.159>.
- Tester, J. W., Anderson, B. J., Batchelor, A. S., Blackwell, D. D., DiPippo, R., Drake, E. M., Garnish, J., Livesay, B., Moore, M. C., Nichols, K., Petty, S., Toksöz, M. N., & Veatch, R. W. (2006). *The future of geothermal energy: Impact of enhanced geothermal systems (EGS) on the United States in the 21st Century*. MIT.
- Toews, M., Riddell, D., Vany, J., & Schwarz, B. (2020). Case study of a multilateral closed-loop geothermal system. In *Proceedings of the world geothermal congress 2020*, Reykjavik, Iceland.
- van der Vaart, J., Bär, K., Frey, M., Reinecker, J., & Sass, I. (2021). Quantifying model uncertainty of a geothermal 3D model of the Cenozoic deposits in the northern Upper Rhine Graben, Germany. *Journal of Applied and Regional Geology. Zeitschrift der Deutschen Gesellschaft für Geowissenschaften*, 172(3), 365–379.
- Weinert, S., Bär, K., & Sass, I. (2020). *Petrophysical properties of the mid-german crystalline high: A database for Bavarian, Hessian, Rhineland-Palatinate and Thuringian Outcrops*. TUDatalib. Retrieved 27 June 2022, from <https://doi.org/10.25534/tudatalib-278>.
- Welsch, B., Göllner-Völker, L., Schulte, D. O., Bär, K., Sass, I., & Schebek, L. (2018). Environmental and economic assessment of borehole thermal energy storage in district heating systems. *Applied Energy*, 216, 73–90.
- Williams, C. F. (2007). Updated methods for estimating recovery factors for geothermal resources. In *Proceedings of the thirty-second workshop on geothermal reservoir engineering*. Stanford, California.
- Williams, C. F., Reed, M. F., & Mariner, R. H. (2008). *A review of methods applied by the U.S. geological survey in the assessment of identified geothermal resources: Open-file report 2008–1296*. USGS.
- Winsloe, R., Richter, A., & Vany, J. (2021). The emerging (and proven) technologies that could finally make geothermal scalable. In *Proceedings of the world geothermal congress 2020*, Reykjavik, Iceland.
- Zeh, A., & Gerdes, A. (2010). Baltica- and Gondwana-derived sediments in the Mid-German Crystalline Rise (Central Europe): Implications for the closure of the Rheic ocean. *Gondwana Research*, 17(2–3), 254–263.
- Ziegler, P. A., Cloetingh, S., & van Wees, J.-D. (1995). Dynamics of intra-plate compressional deformation: The Alpine foreland and other examples. *Tectonophysics*, 252(1–4), 7–59.